

Advanced statistical methods for eye movement analysis and modeling: a gentle introduction

Giuseppe Boccignone

G. Boccignone
Dipartimento di Informatica, Università di Milano
via Comelico 39/41, 10135 Milano, Italy
<http://boccignone.di.unimi.it> e-mail: giuseppe.boccignone@unimi.it

Table of content

Advanced statistical methods for eye movement analysis and modeling: a gentle introduction		1
Giuseppe Boccignone		
1	Summary	4
2	Introduction	4
	2.1 Suggested references	9
3	A probabilistic tour of current computational models of eye movements and visual attention (with some criticism)	12
4	Stochastic processes and eye movements	22
5	How to leave the past behind: Markov Processes	26
	5.1 Case study: the Horowitz and Wolfe hypothesis of amnesic visual search	30
	5.2 Stationary Markov processes and Markov chains	31
	5.2.1 Case study: modeling gaze shifts as observable finite Markov chains	32
	5.3 Levels of representation of the dynamics of a stochastic process	33
	5.3.1 Example: the Wiener process	36
	5.3.2 Case study: from random walks to saccade latency	41
	5.4 Walking on the safe side: the Central Limit Theorem	42
6	Walking on the wild side: eye movements beyond the CLT	44
	6.1 A first violation: i.i.d denied	44
	6.1.1 Case study: random walk analysis of microsaccades	45
	6.1.2 Case study: optokinetic nystagmus	45
	6.2 A second violation: loosing your moments	46
	6.2.1 Case study: the Lévy flight of saccades	51
	6.2.2 Case study: the microsaccade conundrum	52
	6.3 The foraging perspective	53

7	From patterns of movement to patterns of the mind: unveiling observer’s hidden states	55
7.1	Inverting Yarbus to infer the task	57
7.1.1	Case study: Inverting Yarbus via Naïve Bayes	59
7.1.2	Case study: Inverting Yarbus via HMM ..	60
7.2	Assessing cognitive impairments and expertise	61
7.2.1	Case study: Assessing cognitive impairments	62
7.2.2	Case study: Classifying billiard player expertise	63
	References	65

1 Summary

In this Chapter we show that by considering eye movements, and in particular, the resulting sequence of gaze shifts, a stochastic process, a wide variety of tools become available for analyses and modelling beyond conventional statistical methods. Such tools encompass random walk analyses and more complex techniques borrowed from the pattern recognition and machine learning fields.

After a brief, though critical, probabilistic tour of current computational models of eye movements and visual attention, we lay down the basis for gaze shift pattern analysis. To this end, the concepts of Markov Processes, the Wiener process and related random walks within the Gaussian framework of the Central Limit Theorem will be introduced. Then, we will deliberately violate fundamental assumptions of the Central Limit Theorem to elicit a larger perspective, rooted in statistical physics, for analysing and modelling eye movements in terms of anomalous, non-Gaussian, random walks and modern foraging theory.

Eventually, by resorting to machine learning techniques, we discuss how the analyses of movement patterns can develop into the inference of hidden patterns of the mind: inferring the observer’s task, assessing cognitive impairments, classifying expertise.

2 Introduction

Consider Figure 1: it shows typical *scan paths* (in this case a succession of saccades and fixations) produced by two human observers on a natural image: circular spots and lines joining spots graphically represent fixations and gaze shifts between subsequent fixations, respectively.

When looking at scan paths, the first question arising is: How can we characterize the shape and the statistical properties of such trajectories? Answering this question entails a *data analysis* issue. The second question is: What factors determine the shape and the statistical properties? and relates to the *modeling* issue.

From a mere research practice standpoint these two issues need not be related (yet, from a more general theoretical standpoint such attitude is at least debatable). A great deal of research can be conducted by performing an eye tracking experiment based on a specific paradigm, and then analyzing data by running standard statistical tools (e.g., ANOVA) on scan path “features” such as fixation frequency, mean fixation time, mean saccadic amplitudes, scan path length, etc. The “data-driven” attitude can be preserved even in the case where standard tools are abandoned in favor of more complex techniques borrowed from the pattern recognition and machine learning fields; for instance, in the endeavor of inferring or classifying the observer’s mental task or the expertise behind his gaze shifts (e.g., [49, 10]).

In the same vein, it is possible to set up a gaze shift model and successively assess its performance against eye tracking data in terms of classic statistical analyses.

Clearly, the program of following the data lies at the heart of scientific methodology. When trying to understand a complex process in nature, the empirical evidence is essential. Hypotheses must be compared with the actual data, but the empirical evidence itself may have limitations; that is, it may not be sufficiently large or accurate either to confirm or rule out hypotheses, models, explanations, or assumptions, even when the most sophisticated analytical tools are used.

For eye movement patterns, this issue may be in some cases particularly delicate. Such patterns are, in some sense, a summary of all the motor and perceptual activities in which the observer has been involved during data collection. As sketched in Figure 2, from a functional standpoint, there are

Fig. 1 Different scan paths on a pair of images eye-tracked from different human observers. Left, free viewing of a natural scene; right, natural scene embedding a face. The area of yellow disks marking fixations between saccades is proportional to fixation time (images and eye tracking data from the Fixations in FAcEs dataset)



several interacting action / perception loops that drive eye movements. These factors act on different levels of representation and processing: salience, for instance, is a typical bottom-up process, while plans are typical top-down processes

In principle, all such activities should be taken into account when analyzing and modeling actual eye movements in visual attention behavior. Clearly, this is a mind-blowing endeavour.

This raises the question of what is a computational model and how it can support more advanced data analysis of experimental data. In this Chapter we discuss a minimal phenomenological model.

At the most general level, the aim of a computational model of visual attention is to answer the question *Where to Look Next?* by providing:

1. at the *computational theory level* (in the sense of Marr, [68]; defining the input/output computation at time t), an account of the mapping from visual data of a complex natural scene, say \mathcal{D} (raw image data, or more usefully, features), to a sequence of gaze locations $\mathbf{x}_F(1), \mathbf{x}_F(2), \dots$, under a given task \mathbf{T} , namely

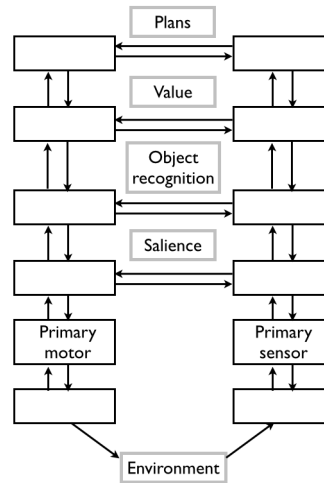
$$\mathcal{D} \xrightarrow{\mathbf{T}} \{\mathbf{x}_F(1), \mathbf{x}_F(2), \dots\}, \quad (1)$$

where the sequence $\{\mathbf{x}_F(1), \mathbf{x}_F(2), \dots\}$ can be used to define a scan path (as illustrated in Figure 3);

2. at the *algorithmic level*, [68], a procedure that simulates such mapping (we will not specifically address here the third level of neural realisation [68]).

Under this conceptualization, when considering for instance the input \mathcal{D} in the form of a static scene (a picture), either the raw time series

Fig. 2 Framework for the control of eye movements. There are several interacting layers of control that influence target selection: the scheme highlights, top to bottom, the contributions of plans, value, object recognition and salience to target selection. The left-hand route summarizes the motor components, the right hand, the perceptual components. Figure modified after Schütz *et al* [93]



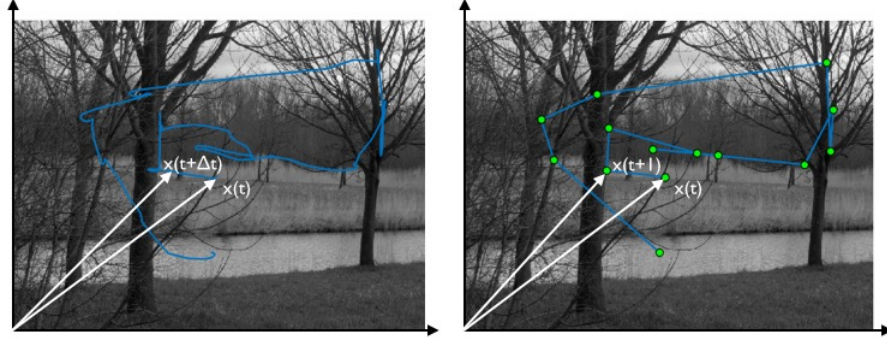


Fig. 3 Scan path of an eye-tracked human observer rendered as a temporal sequence of gaze position represented by time-varying location vectors $\mathbf{x}(t)$. The Left image shows the continuous raw-data trajectory; the right image, the discretized sequence of fixations and saccades. Images and data are from the Doves dataset [106], which is freely available on the Web

$\{\mathbf{x}_F(1), \mathbf{x}_F(2), \dots\}$ or fixation duration and saccade (length and direction) are the only two observable behaviors of the underlying control mechanism. When, \mathcal{D} is a dynamic or time varying scene (e.g. a video), then pursuit needs to be taken also into account, and we can adopt more the generic terms of gaze shifts (either pursuit or saccades) and gaze shift amplitudes. Fixation duration and shift amplitude vary greatly during visual scanning of the scene. As previously discussed, such variation reflects moment-to-moment changes in the visual input, processes occurring at different levels of representation, the state of the oculomotor system and stochastic variability in neuromotor force pulses.

We can summarize this state of affairs by stating that fixation duration and the time series $\{\mathbf{x}_F(1), \mathbf{x}_F(2), \dots\}$ (or equivalently, gaze shift lengths and directions) are random variables (RVs) that are generated by an underlying random process. In other terms, the sequence $\{\mathbf{x}_F(1), \mathbf{x}_F(2), \dots\}$ is the realization of a stochastic process, and the goal of a computational theory is to develop a mathematical model that describes statistical properties of eye movements as closely as possible.

Is this minimalist approach to computational modeling of gaze shifts a reasonable one? The answer can be positive if “systematic tendencies” between fixation durations, gaze shift amplitudes and directions of successive eye movements exist and such sequential dependencies can be captured by the stochastic process model. Systematic tendencies in oculomotor behaviour can be thought of as regularities that are common across all instances of, and manipulations to, behavioural tasks. In that case useful information about how the observers will move their eyes can be found.

Indeed, such systematic tendencies or “biases” in the manner in which we explore scenes with our eyes are well known in the literature. One example

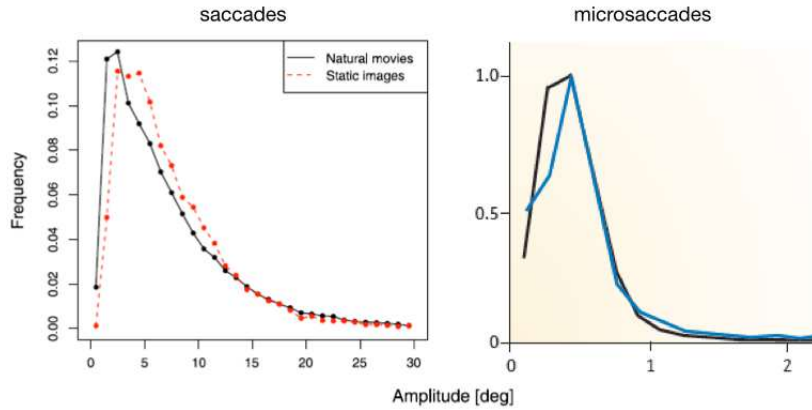


Fig. 4 Amplitudes distribution of saccades (on natural movies and static images, left) and microsaccades (right, recordings via video - black - and search coil - blue). In both cases amplitudes follow a positively skewed, long-tailed distribution. Figure modified after Dorr *et al* [31] and Martinez-Conde *et al* [69]

is provided in Figure 4 showing the amplitude distribution of saccades and microsaccades that typically exhibit a positively skewed, long-tailed shape. Other paradigmatic examples of systematic tendencies in scene viewing are [100, 101]: initiating saccades in the horizontal and vertical directions more frequently than in oblique directions; small amplitude saccades tending to be followed by long amplitude ones and vice versa.

Such biases may arise from a number of sources. Tatler and Vincent [101] have suggested the following: biomechanical factors, saccade flight time and landing accuracy, uncertainty, distribution of objects of interest in the environment, task parameters.

Understanding biases in how we move the eyes can provide powerful new insights into the decision about where to look in complex scenes. In a remarkable study [101], Tatler and Vincent have shown that a model based solely on these biases and therefore blind to current visual information can outperform salience-based approaches.

Clearly, the adoption of an approach based on stochastic processes can benefit of all the analysis and modeling tools that have been developed within such field and in the field of time series, much like happened to modern developments of econophysics [66] and finance [79].

But further, this open the possibility of treating visual exploration strategies in terms of *random walks*, e.g., [36, 37, 18] and, most interesting, of *foraging* strategies [14, 113, 16, 4, 8, 24].

In this Chapter, we pursue the following learning objectives

1. Casting eye movement analysis and modeling in probabilistic terms (Section 3);

2. Understanding the essential concepts of stochastic process, such as Markov processes, and microscopic/macroscopic levels of description (Sections 4, 5);
3. Setting the basics of random walk analyses and modelling of eye movements either within the scope of the Central Limit Theorem or beyond, towards anomalous walks and diffusions (Sections 6);
4. Moving from the analyses of scan path patterns to the inference of mental patterns by introducing the basic tools of modern probabilistic Machine learning (Section 7).

2.1 Suggested references

As to the concepts in the modelling review of the next Section, it is worth referring to some of the Chapters of this book. In particular [to be completed.....]

For all the topics covered in this Chapter we assume a basic calculus level or at least a familiarity with the concepts of differentiation and integration. Table 1 provides a brief introductory note. However, find an A-level text book with some diagrams if you have not seen this before. Similarly, we surmise reader’s conversance with elementary notions of probability and statistics.

To explore beyond the contents of this Chapter, we recommend the following. A brief and clear introduction to stochastic processes (from a physicist’s point of view) can be found in a few chapters of Huang’s “Introduction to statistical physics” [53]. A comprehensive treatment of stochastic processes is given in Gardiner’s “Stochastic Methods: A Handbook for the Natural and Social Sciences” [42]; it is a great starting point if you are looking for specific information about a specific stochastic process. One of the finest books on stochastic processes is van Kampen’s classic “Stochastic processes in physics and chemistry” [107]; difficult reading, but well-worth the effort. A modern treatment of the subject is provided in Paul and Baschnagel “Stochastic Processes – From Physics to Finance” [79], with a clear discussion of what happens beyond the Central Limit Theorem.

A beautiful bridge between stochastic processes and foraging is outlined in Méndez, Campos, and Bartumeus, “Stochastic Foundations in Movement Ecology: Anomalous Diffusion, Front Propagation and Random Searches” [70]. However, if one wants to skip more technical details, an affordable, easy to read introduction to foraging and Lévy flights is “The physics of foraging” by Viswanathan *et al.* [109].

Eventually, for what concerns statistical Machine Learning, which is nowadays a vast field, a thorough and simple introduction is provided by Rogers and Girolami [90]. The most comprehensive and up-to-date textbook is that by Kevin Murphy [72].

Table 1 Interlude: differential and integral calculus with no pain

Differential calculus deals with the concept of **rate of change**. The rate of change of a function $f(x)$ is defined as the ratio of the change in f to the change in x . Consider Fig.5 showing a plot of f as a function of x there are intervals during which f increases and other intervals during which f decreases. We can quantify the ups and downs of the changes in the values of f by estimating the slope, i.e., the change in the variable f over a given interval Δx , say between x_1 and x_2 . Denote the interval or average slope by

$$\frac{\Delta f}{\Delta x} = \frac{f(x_2) - f(x_1)}{x_2 - x_1} = \frac{f(x + \Delta x) - f(x)}{\Delta x} = \frac{\text{rise}}{\text{run}},$$

with $\Delta x = x_2 - x_1$. What happens as the interval Δx becomes smaller and smaller and approaches zero, formally, $\Delta x \rightarrow 0$?

In that case the interval or average rate of change shrinks to the *instantaneous rate of change*. This is exactly what is computed by the derivative of f

$$\frac{df}{dx} = \lim_{\Delta x \rightarrow 0} \frac{f(x + \Delta x) - f(x)}{\Delta x}.$$

If you prefer thinking in a geometric way, the derivative at a point x provides the slope of the tangent of the curve at x .

As an example, we calculate the derivative of the function $f(x) = x^2$. First, write the term $f(x + \Delta x)$:

$$f(x + \Delta x) = (x + \Delta x)^2 = x^2 + 2x\Delta x + \Delta x^2$$

Then, subtract $f(x)$ and divide by Δx :

$$\frac{f(x + \Delta x) - f(x)}{\Delta x} = \frac{x^2 + 2x\Delta x + \Delta x^2 - x^2}{\Delta x} = 2x + \Delta x$$

Now in the limit $\Delta x \rightarrow 0$ we shrink Δx to zero, i.e.,

$$\lim_{\Delta x \rightarrow 0} 2x + \Delta x = 2x.$$

Eventually,

$$\frac{d(x^2)}{dx} = 2x.$$

If differential calculus has to do with rates of change, **integral calculus** deals with sums of many tiny incremental quantities. For instance, consider a continuous function f such as the one plotted in Fig. 6 and the following sum

$$\sum_{i=1}^n f(x_i)\Delta x = f(x_1)\Delta x + f(x_2)\Delta x + \cdots + f(x_n)\Delta x.$$

Here the uppercase greek letter \sum indicates a sum of successive values defined by i and where $\Delta x = \frac{b-a}{n}$ and $x_i = a + i\Delta x$. Note that the term

$$f(x_i)\Delta x = \text{height} \times \text{width} = \delta A_i$$

computes the area δA_i of the i -th rectangle (see Fig. 6). Thus, the (Riemann) sum written above approximates the area defined by the continuous function f within the left and right limits a and b , as a the sum of tiny rectangles covering the area under f . The sum transforms into the (Riemann) integral

$$\int_a^b f(x)dx = \lim_{\Delta x \rightarrow 0} \sum_{i=1}^n f(x_i)\Delta x$$

when Δx shrinks to 0 (i.e. in the limit $\Delta x \rightarrow 0$) and the number n of intervals grows very large ($\Delta n \rightarrow \infty$).

There is a deep connection between integration and differentiation, which is stated by the *fundamental theorem of calculus*: the processes of integration and differentiation are reciprocal, namely, the derivative of an integral is the original integrand.

Table 2 Visual attention models: a brief critical review

In the field of psychology, there exists a wide variety of theories and models on visual attention (see, e.g., the review by Heinke and Humphreys [48]). Among the most influential for computational attention systems, the well known Treisman's Feature Integration Theory (FIT) [104, 103], Wolfe's Guided Search Model [112] aiming at explaining and predicting the results of visual search experiments, Desimone and Duncan's Biased Competition Model (BCM, [30]), Rensink's triadic architecture [87], and the Koch and Ullman's bottom-up model [59].

Other psychophysical models have addressed attention modelling in a more formal framework. One notable example is Bundesen's Theory of Visual Attention (TVA, [15]), further developed by Logan into the CODE theory of visual attention (CTVA, [63]). Also, theoretical approaches to visual search have been devised by exploiting Signal Detection Theory [78].

At a different level of explanation, other proposals have been conceived in terms of connectionist models, such as MORSEL (Multiple Object Recognition and attentional SElection, [71]), SLAM (SeLective Attention Model) [80], SERR (SEarch via Recursive Rejection) [54], and SAIM (Selective Attention for Identification Model by Heinke and Humphreys [47]) subsequently refined in the Visual Search SAIM (VS-SAIM) [46].

To a large extent, the psychological literature was conceived and fed on simple stimuli, nevertheless the key role that the above models continue to play in understanding attentive behaviour should not be overlooked. For example, many current computational approaches, by and large, build upon the bottom-up salience based model by Itti *et al.* [55], which in turn is the computational counterpart of Koch and Ullman and Treisman's FIT models. The seminal work of Torralba *et al.* [102], draws on an important component of Rensink's triadic architecture [87], in that it considers contextual information such as gist - the abstract meaning of a scene, e.g., a city scene, etc. - and layout - the spatial arrangement of the objects in a scene. More recently, Wischniewski *et al.* [111] have presented a computational model that integrates Bundesen's TVA [15].

However, in the last three decades, psychological models have been adapted and extended in many respects, within the computational vision field where the goal is to deal with attention models and systems that are able to cope with natural complex scenes rather than simple stimuli and synthetical images (e.g., see [41] and the most recent review by Borji and Itti [12]). The adoption of complex stimuli has sustained a new brand of computational theories, though this theoretical development is still at an early stage: up to this date, nobody has really succeeded in predicting the sequence of fixations of a human observer looking at an arbitrary scene [41]. This is not surprising given the complexity of the problem. One might think that issues of generalisation from simple to complex contexts are nothing more than a minor theoretical inconvenience; but, indeed, the generalisation from simple to complex patterns might not be straightforward. As it has been noted in the case of attentive search, a model that exploits handpicked features may fail utterly when dealing with realistic objects or scenes [115].

Current approaches within this field suffer from a number of limitations: they mostly rely on a low-level salience based representation of the visual input, they seldom take into account the task's role, and eventually they overlook the eye guidance problem, in particular the actual generation of gaze-shifts (but see Tatler *et al* [99] for a lucid critical review of current methods). We will discuss such limitations in some detail in Section 3.

Fig. 5 A plot of the values of a function f as a function of x , showing a region of negative rate of change or slope (between x_1 and x_2) and a region of positive change (between x_3 and x_4).

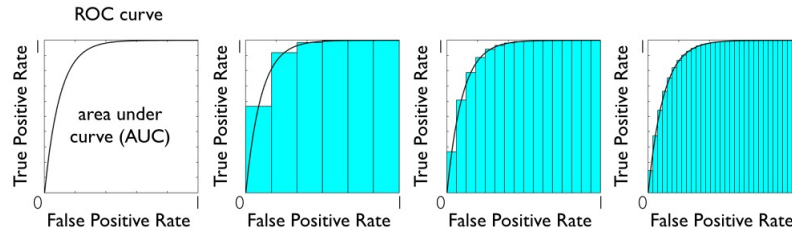
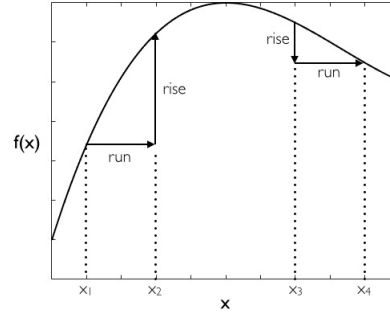


Fig. 6 An illustration of the integral concept by using Receiver Operating Characteristic (ROC) analysis, one of the methods to evaluate saliency map algorithms. Continuous saliency maps are processed as a binary classifier applied on every pixel: the image pixels of the ground truth, as well as those of the prediction, are classified as fixated (or salient) or as not fixated (not salient). A simple threshold operation is used for this purpose. The ROC curve is exploited to display the classification result for a varying threshold used, each threshold value originating a number of False Positives and True Positives. An ROC curve is shown in the leftmost graph, and it has been obtained by plotting the False Positive Rate (FPR) as a function of the True Positive Rate (TPR). The ROC area, or the area under curve (AUC), provides a measure indicating the overall performance of the classification. The second graph shows the approximate calculus of the AUC as the (Riemann) sum of approximating rectangles as discussed in Table 1. Third and fourth graphs demonstrate how the computed AUC becomes more and more precise for increasing number of rectangles ($\Delta n \rightarrow \infty$) and diminishing rectangle widths ($\Delta x \rightarrow 0$). In such limit the sum \sum becomes the integral \int .

3 A probabilistic tour of current computational models of eye movements and visual attention (with some criticism)

Many models in psychology and in the computational vision literature have investigated limited aspects of the problem of eye movements in visual attention behavior (see Table 2, for a quick review). And, up to now, no model has really succeeded in predicting the sequence of fixations of a human observer looking at an arbitrary scene [41].

Table 3 Dangerous relationships: A rendezvous with Bayesian Probabilities

We assume the readers to be already familiar with the elementary notions (say, undergrad level) of probability and **random variables** (RVs). Thus, a warning. Sometimes we talk about probabilities of events that are “out there” in the world. The face of a flipped coin is one such event. But sometimes we talk about probabilities of events that are just possible beliefs “inside the head.” Our belief about the fairness of a coin is an example of such an event. Clearly, it might be bizarre to say that we randomly sample from our beliefs, like we sample from a sack of coins. To cope with such embarrassing situation, we shall use probabilities to express our information and beliefs about unknown quantities. $P(A)$ denotes the probability that the event A is true. But event A could stand for logical expressions such as “there is red car in the bottom of the scene” or “an elephant will enter the pub”. In this perspective, probability is used to quantify our uncertainty about something; hence, it is fundamentally related to information rather than repeated trials. Stated more clearly: we are adopting the Bayesian interpretation of probability in this Chapter.

Fortunately, the basic rules of probability theory are the same, no matter which interpretation is adopted (but not that smooth, if we truly addressed inferential statistics). For what follows, in this chapter we just need to refresh a few.

Let X and Y be RVs. In Bayesian inference a RV (either discrete or continuous) is defined as an unknown numerical quantity about which we make probability statements. For example, the quantitative outcome of a survey, experiment or study is a RV. Call $P(X, Y)$ their joint probability. The conditional probability of X given Y is:

$$P(X | Y) \equiv \frac{P(X, Y)}{P(Y)} \text{ if } P(Y) \neq 0. \quad (2)$$

In Bayesian probability we always have conditional probabilities, at least we condition on the assumptions or set of hypotheses \mathcal{H} on which the probabilities are based. In data modeling and Machine Learning, the following holds [64]:

You cannot do inference without making assumptions

Then, the rules below will be useful:

Product rule (or chain rule)

$$P(X, Y | \mathcal{H}) = P(X | Y, \mathcal{H})P(Y | \mathcal{H}) \quad (3)$$

Sum rule (marginalization)

$$P(Y | \mathcal{H}) = \sum_X P(X, Y | \mathcal{H}) \text{ (discrete RVs)} \quad (4)$$

$$P(Y | \mathcal{H}) = \int_X P(X, Y | \mathcal{H})dX \text{ (continuous RVs)} \quad (5)$$

Bayes’ rule (see Fig. 7 for a simple example)

$$P(X | Y, \mathcal{H}) = \frac{P(Y | X, \mathcal{H})P(X | \mathcal{H})}{P(Y | \mathcal{H})} \leftrightarrow \text{posterior} = \frac{\text{likelihood} \times \text{prior}}{\text{evidence}} \quad (6)$$

To avoid burying the reader under notations, we have used $P(\cdot)$ to denote both the probability of a discrete outcome (**probability mass**) and the probability of a continuous outcome (**probability density function**, pdf). We let context make things clear. Also, for more fine-grained events we may adopt the form $X = x$ for a specific choice of value (outcome) of the RV X . Briefer notation will sometimes be used. For example, $P(X = x)$ may be written as $P(x)$ or $P(X)$. A bold \mathbf{X} might denote a set of RVs or a random vector/matrix.

The “bible” of the Bayesian approach is the treatise of Jaynes [56]. A succinct introduction with an eye to inference and learning problems can be found in Chapter 2 of the beautiful book by MacKay [64], which is also available for free online, <http://www.inference.phy.cam.ac.uk/mackay/itila/>. The Bayesian world is not a small world: more resources are listed at <http://bayesian.org/publications/books>.

The issue of devising a computational model of eye guidance as related to visual attention - i.e. answering the question *Where to Look Next?* in a formal way - can be set in a probabilistic Bayesian framework (see Table 3 for a brief introduction). Tatler and Vincent [101] have re-phrased this question in terms of Bayes' rule:

$$\underbrace{P(\mathbf{x} | \mathcal{D})}_{\text{posterior prob. of gaze shift}} = \frac{\overbrace{P(\mathcal{D} | \mathbf{x})}^{\text{data likelihood under the shift}}}{P(\mathcal{D})} \underbrace{P(\mathbf{x})}_{\text{gaze shift prior}}, \quad (7)$$

where $\mathbf{x} = \mathbf{x}_F(t) - \mathbf{x}_F(t-1)$ is the random vector representing the gaze shift (in [101], saccades), and \mathcal{D} generically stands for the input data. As Tatler and Vincent put it, "The beauty of this approach is that the data could come from a variety of data sources such as simple feature cues, derivations such as Itti's definition of salience, object-or other high-level sources".

In Eq. 7, the first term on the r.h.s. accounts for the likelihood of particular visual data (e.g., features, such as edges or colors) occurring at a gaze shift target location normalized by $P(\mathcal{D})$ the pdf of these visual data occurring in the environment. As we will see in brief, this first term bears a close resemblance to approaches previously employed to evaluate the possible involvement of visual features in eye guidance.

Most interesting, and related to issues raised in the introductory Section, is the Bayesian prior $P(\mathbf{x})$, i.e., the probability of shifting the gaze to a location *irrespective of the visual information* at that location. Indeed, this term will encapsulate any systematic tendencies in the manner in which we explore scenes with our eyes. The striking result obtained by Tatler and Vincent [101] is that if we learn $P(\mathbf{x})$ from actual observer's behavior, then we can **sample** gaze shifts (cfr. Table 4), i.e.,

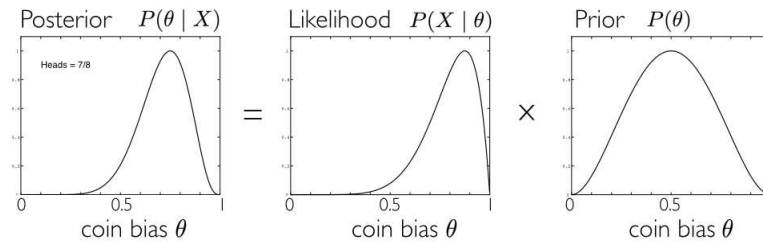


Fig. 7 An illustration of the use of the Bayes' rule for inferring the bias of a coin on the basis of coin tossing results. The prior probability $P(\theta)$ for the coin bias θ captures the assumption that the coin is likely to be a fair one (the pdf is "peaked" on $\theta = 0.5$). However, 7 heads occur after 8 tosses. Such experimental result is captured by the shape of the likelihood $P(X | \theta)$ strongly biased to the right. Bayes' rule computes the posterior pdf $P(\theta | X)$ by "updating" the initial prior through the "observed" likelihood (the evidence term is not shown in the figure and it has been treated as a normalization factor to constrain probabilities between 0 and 1)

$$\mathbf{x}(t) \sim P(\mathbf{x}), \quad t = 1, 2, \dots \quad (8)$$

so to obtain scan paths that, blind to visual information, out-perform feature-based accounts of eye guidance: 0.648 area under the receiver operator curve (AUC, which has been illustrated in Fig. 6) as opposed to 0.593 for edge information and 0.565 for salience information [101].

Table 4 When God plays dice: the art (and magic) of sampling

Eye movements can be considered a natural form of sampling. Another example of actual physical sampling is tossing a coin, as in the example illustrated in Fig. 8, or throwing dice. Nevertheless, we can (and need to) **simulate** sampling that occurs in nature (and thus the underlying process). Indeed, for both computational modelling and analysis we assume of being capable of the fundamental operation of generating a sample $\mathbf{X} = \mathbf{x}$ from a probability distribution $P(\mathbf{X})$. We denote the sampling action via the \sim symbol:

$$\mathbf{x} \sim P(\mathbf{X}). \quad (9)$$

For instance, tossing a coin like we did in the example of Fig. 7 can be simulated by sampling \mathbf{x} from a **Bernoulli distribution**, $\mathbf{x} \sim \text{Bern}(\mathbf{X}; \theta)$, where θ is the parameter standing for the coin bias.

Surprisingly, to simulate nature, we need a minimal capability: that of generating realisations of RVs uniformly distributed on the interval $[0, 1]$. In practical terms, we just need a programming language or a toolbox in which a `rand()` function is available implementing the $\mathbf{u} \sim \text{Uniform}(0, 1)$ operation. Indeed, given the RVs \mathbf{u} , we can generate the realisations of any other RV with appropriate “transformations” of \mathbf{u} .

There is a wide variety of “transformations” for generating samples, from simple ones (e.g. inverse transform sampling and rejection sampling) to more sophisticated, like those relying on **Markov Chain Monte Carlo** methods (e.g., **Gibbs sampling** and **Metropolis sampling**). Again, MacKay’s book [64] provides a very clear introduction to the art of random sampling.

You can qualitatively assess the results of your computational sampling procedure using sample **histograms**. Recall from your basic statistic courses that an histogram is an empirical estimate of the probability distribution of a continuous variable. It is obtained by “binning” the range of values – that is, by dividing the entire range of values into a series of small intervals –, and then counting how many values fall into each interval. Intuitively, if we look at the empirical distribution of the set of samples $\{\mathbf{x}(t)\}_{t=1}^T$ obtained for a large number T of sampling trials $\mathbf{x}(t) \sim P(\mathbf{X})$, $t = 1, 2, \dots, T$, we expect the shape of the histogram to approximate the originating theoretical density. Examples are provided in Fig. 8 where 1000 samples have been generated experimenting with the **Uniform distribution**, the **Gaussian distribution** and the **Cauchy distribution**, respectively.

Learning is basically obtained by empirically collecting through eye tracking the observer’s behavior on an image data set (formally, the joint pdf $P(\mathbf{x}, \mathcal{D})$) and then factoring out the informative content of the specific images, briefly, via marginalization, i.e., $P(\mathbf{x}) = \sum_{\mathcal{D}} P(\mathbf{x}, \mathcal{D})$.

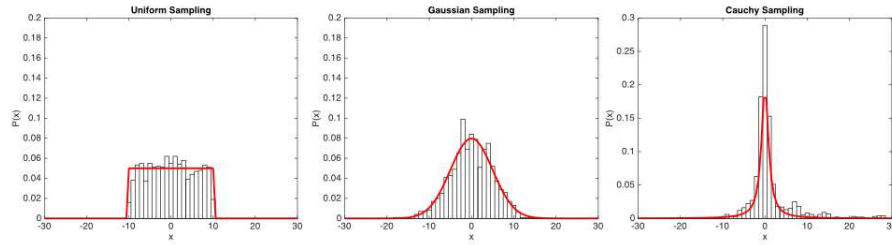
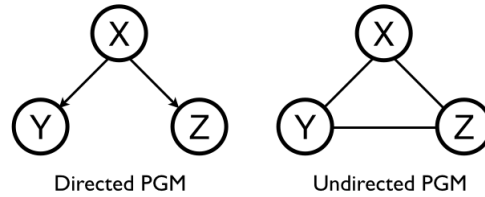


Fig. 8 From left to right, the empirical distributions (histograms) for $n = 1000$ samples drawn from Uniform, Gaussian and Cauchy pdfs. Uniform and Gaussian sampling have been performed via the Matlab functions `rand()` and `randn()`, respectively; samples from the Cauchy pdf have been generated resorting to Metropolis sampling. Each histogram is overlaid with the generating theoretical density depicted as a continuous red curve

Fig. 9 Probabilistic Graphical Models: a directed PGM (left, a.k.a. Bayesian Network) and an undirected PGM (right, a.k.a. Markov Random Field). Nodes represent RVs and arcs express probabilistic relationships between RVs



Note that the apparent simplicity of the prior term $P(\mathbf{x})$ hides a number of subtleties. For instance, Tatler and Vincent expand the random vector \mathbf{x} in terms of its components, amplitude l and direction θ . Thus, $P(\mathbf{x}) = P(l, \theta)$. This simple statement paves the way to different options. First easy option: such RVs are marginally independent, thus, $P(l, \theta) = P(l)P(\theta)$. In this case, gaze guidance, solely relying on biases, could be simulated by expanding Eq. 8 via independent sampling of both components, i.e. at each time t , $l(t) \sim P(l(t)), \theta(t) \sim P(\theta(t))$. Alternative option: conjecture some kind of dependency, e.g. amplitude on direction so that $P(l, \theta) = P(l | \theta)P(\theta)$. In this case, the gaze shift sampling procedure would turn into the sequence $\hat{\theta}(t) \sim P(\theta(t)), l(t) \sim P(l(t) | \theta(t))$. Further: assume that there is some persistence in the direction of the shift, which give rise to a stochastic process in which subsequent directions are correlated, i.e., $\theta(t) \sim P(\theta(t) | \theta(t-1))$, and so on.

To summarize, by simply taking into account the prior $P(\mathbf{x})$, a richness of possible behaviors and analyses are brought into the game. Unfortunately, most computational accounts of eye movements and visual attention have overlooked this issue. We noticed before, by inspecting Eq. 7 that the term $\frac{P(\mathcal{D}|\mathbf{x})}{P(\mathcal{D})}$ bears a close resemblance to many approaches proposed in the literature. This is an optimistic view. Most of the approaches actually discard the dynamics of gaze shifts, say $\mathbf{x}_F(t) \rightarrow \mathbf{x}_F(t+1)$, implicitly captured through

Table 5 Probabilistic Graphical Models (PGM)

A PGM [60] is a graph-based representation (see Figure 9) where **nodes** (also called vertices) are connected by **arcs** (or **edges**). In a PGM, each node represents a RV (or group of RVs), and the arcs express probabilistic relationships between these variables. When arcs are shaped as arrows, such relations represent a conditional dependency (Figure 9, left). For instance the structural dependency $X \rightarrow Y$, states the probabilistic dependency of RV Y on X represented via the conditional probability $P(Y|X)$. It is important to note that arrows do not generally represent causal relations, though in some circumstances it could be the case. Graphs that have a directionality indicated by arrows are **directed** PGM, a generalization of **Bayesian Networks** (BN), well known in the Artificial Intelligence community. The other major class of PGMs are **undirected** PGM (Figure 9, right), in which the links do not carry arrows and have no directional significance, but are suitable to express soft constraints between RVs. The latter are also known as **Markov Random Fields** (MRF), largely exploited in Computer Vision. In this Chapter, we shall focus on directed PGM representations.

We will mainly exploit PGMs as a descriptive tool, because they offer several useful properties : 1) they provide a simple way to visualize the structure of a probabilistic model and can be used to design and motivate new models; 2) they offer insights into the properties of the model, including conditional independence properties, which can be obtained by inspection of the graph.

In particular, the graph captures the way in which the joint distribution over all of the RVs can be decomposed into a product of factors each depending only on a subset of the variables. Consider the example presented in Figure 10. We want to describe a simple object-based attention model in which we deal with objects (e.g., red triangles vs. blue squares), their possible locations, and the visual features we sense from the observed scene. At the most general level, such “world” can be described by the “probability of everything”, the joint pdf $P(\text{Objects}, \text{Location}, \text{Features})$ which we denote, more formally, through the RVs O, L, F :

$$P(\text{Objects}, \text{Location}, \text{Features}) \equiv P(O, L, F). \quad (10)$$

Recall that via the product rule, the joint pdf could be factorized in a (combinatorial) variety of ways, all equivalent and admissible:

$$\begin{aligned} P(O, L, F) &= P(O | L, F)P(L | F)P(F) \\ &= P(L | O, F)P(O | F)P(F) \\ &= P(F | O, L)P(O | L)P(L) \\ &= \dots \end{aligned} \quad (11)$$

However, from our experience, we recognize the third factorization as the most meaningful one: the likelihood of observing certain features (e.g, color) in the visual scene depends on *what* kind of objects are present and *where* they are located; thus, the factor $P(F | O, L)$ makes sense. $P(L)$ represents the prior probability of choosing certain locations within the scene (e.g., it could code the center bias effect [97]). Eventually, the $P(O | L)$ factor might code the prior probability of certain kinds of objects (e.g., we may live in a world where red triangles are more frequent than blue squares). As to $P(O | L)$ we can further assume that the object location and object identity are independent, Formally, $P(O | L) = P(O)$, finally leading to the following simplified factorization:

$$P(O, L, F) = P(F | O, L)P(O)P(L) \quad (12)$$

This factorization is exactly that captured by the structure of the directed PGM presented in Figure 10.

For the purpose of this Chapter this is just what we need. But further, we could “query” the PGM for making any kind of probabilistic inference. For instance, we could ask what is the (posterior) probability of observing certain objects at certain locations given the observed features:

$$P(O, L | F) = \frac{P(F | O, L)P(O)P(L)}{P(F)} \quad (13)$$

Note, *en passant*, that the pdf $P(O, L | F)$ in Eq. 13, formalizes the notion of a top-down, object-based salience map. Indeed, complex computations, required to perform inference and learning in sophisticated probabilistic models, can be expressed in terms of graph-based algorithms. PGMs are a formidable tool to such end, and nowadays are widely adopted in modern probabilistic **Machine Learning** and **Pattern Recognition**. An affordable introduction can be found in Bishop [3].

the shift vector $\mathbf{x}(t)$. In practice, most models are more likely to be described by a simplified version of Eq. 7:

$$\underbrace{P(\mathbf{x}_F | \mathcal{D})}_{\text{posterior prob. of gazing at}} = \frac{\underbrace{P(\mathcal{D} | \mathbf{x}_F)}_{\text{data likelihood under gaze at}}}{P(\mathcal{D})} \underbrace{P(\mathbf{x}_F)}_{\text{prior prob. of gazing at}}, \quad (14)$$

By careful inspection, it can be noted that the posterior $P(\mathbf{x}_F | \mathcal{D})$ answers the query ‘‘What is the probability of *fixating* location \mathbf{x}_F given visual data \mathcal{D} ?’. Further, the prior $P(\mathbf{x}_F)$ accounts for the probability of *fixating* location \mathbf{x}_F irrespective of the visual information at that location. The difference between Eq. 7 and Eq. 14 is subtle. But, as a matter of fact, Eq. 14 bears no dynamics. In probabilistic terms we may re-phrase this result as the outcome of an assumption of independence:

$$P(\mathbf{x}) = P(\mathbf{x}_F(t) - \mathbf{x}_F(t - 1)) \simeq P(\mathbf{x}_F(t) | \mathbf{x}_F(t - 1)) = P(\mathbf{x}_F(t)).$$

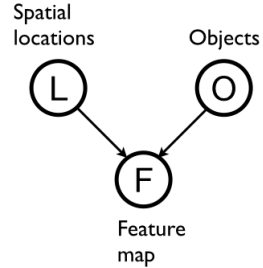
To make things even clearer, let us explicitly substitute \mathbf{x}_F with a RV \mathbf{L} denoting locations in the scene, and \mathcal{D} with RV \mathbf{F} denoting features (whatever they may be); then Eq. 14 boils down to the the following

$$\underbrace{P(\mathbf{L} | \mathbf{F})}_{\text{posterior prob. of selecting location L}} = \frac{\underbrace{P(\mathbf{F} | \mathbf{L})}_{\text{feature likelihood under location L}}}{P(\mathbf{F})} \underbrace{P(\mathbf{L})}_{\text{prior prob. of location L}} \quad (15)$$

The feature-based **Probabilistic Graphical Model** underlying this query (see Table 5 for a brief PGM overview) is a very simple one and is represented on the left of Figure 11. As it can be seen, it is a subgraph of the object-based model PGM (Figure 11, center), which is the one previously discussed in Table 5 (compare to Figure 10).

Surprisingly enough, this simple model is sufficiently powerful to account for a large number of visual attention models that have been proposed in computational vision. This can be easily appreciated by setting $P(\mathbf{F} | \mathbf{L}) = \text{const.}$, $P(\mathbf{L}) = \text{const.}$ so that Eq. 15 reduces to

Fig. 10 A directed PGM capturing the probabilistic relationships among objects (O), spatial locations (L) and observable features (F). Figure modified after Dorr *et al* [31] and Martinez-Conde *et al* [69]



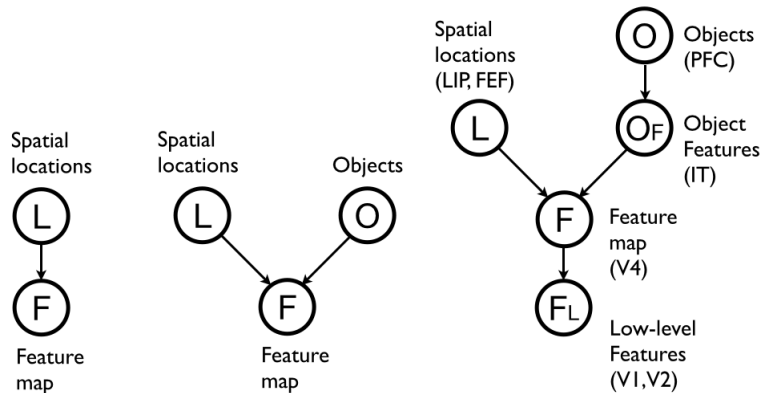


Fig. 11 PGMs of increasing level of representational complexity (left to right) that can account for most models proposed in the computational vision field. Left: feature-based. Center: object-based. Right: the Bayesian model by Chikkerur *et al.* [23], which maps the PGM structure to brain areas underpinning visual attention: early visual areas V1 and V2, V4, lateral intraparietal (LIP), frontal eye fields (FEF), inferotemporal (IT), prefrontal cortex (PFC).

$$\underbrace{\text{posterior prob. of selecting location } \mathbf{L}}_{P(\mathbf{L} | \mathbf{F})} \propto \underbrace{\text{saliency at location } \mathbf{L}}_{\frac{1}{P(\mathbf{F})}}. \quad (16)$$

Eq. 16 tells that the probability of fixating a spatial location $\mathbf{L} = (x, y)$ is higher when “unlikely” features ($\frac{1}{P(\mathbf{F})}$) occur at that location. In a natural scene, it is typically the case of high contrast regions (with respect to either luminance, color, texture or motion) and clearly relates to entropy and information theory concepts [9]. This is nothing but the most prominent saliency-based model in the literature proposed by Itti *et al* [55], which Eq. 16 re-phrases in probabilistic terms.

A thorough reading of the recent review by Borji and Itti [12] is sufficient to gain the understanding that a great deal computational models so far proposed are much or less variations of this leitmotif (experimenting with different features, different weights for combining them, etc.). The weakness of such a pure bottom-up approach has been largely discussed (see, e.g. [99, 40, 32]). Indeed, the effect of early saliency on attention is likely to be a correlational effect rather than an actual causal one [40, 93], though saliency may be still more predictive than chance while preparing for a memory test as discussed by Foulsham and Underwood [40].

Thus, recent efforts have tried to go beyond this simple stage with the aim of climbing the representational hierarchy shown in Figure 2. This entails a first shift from Eq. 16 (based on a oversimplified representation) back to Eq. 15. Torralba *et al.* [102] have shown that using prior knowledge on the typical spatial location of the search target, as well as contextual informa-

tion (the “gist” of a scene) to modulate early saliency improves its fixation prediction.

Next shift is exploiting object knowledge for top-down “tuning” early saliency; thus, moving to the PGM representation at the center of Figure 11. As discussed by Einhäuser *et al.* [32], objects predict fixations in individual images better than early saliency. Indeed, objects and their semantic value have been deemed as fundamental for visual attention and eye guidance (e.g., [71, 15, 87, 46], but see Scholl [92] for a review). For instance, when dealing with faces within the scene, a face detection step can provide a reliable cue to complement early conspicuity maps, as it has been shown by Cerf *et al* [20], deCroon *et al* [29], Marat *et al* [67], or a useful prior for Bayesian integration with low level cues [11]. This is indeed an important issue since faces may drive attention in a direct fashion [19]. The same holds for text regions [20, 24] Other notable exceptions are those provided by Rao *et al.* [85], Sun *et al.* [96], the Bayesian models discussed by Borji *et al.* [13] and Chikkerur *et al.* [23]. In particular the model by Chikkerur *et al.*, which is shown at right of Figure 11 is the most complete to the best of our knowledge (though it does not consider contextual scene information [102], but the latter could be easily incorporated). The authors also have the merit of making the effort of providing links between the structure of the PGM and the brain areas that could support computations.

Further, again in the effort of climbing the representational hierarchy (Figure 2), attempts have been made for incorporating task and value information (see [24, 93] for a brief review, and [99] for a discussion).

Now, a simple question arises: where have the eye movements gone?

To summarize the brief overview above, the common practice of computational approaches is to conceive the mapping (1), as a two step procedure:

1. obtain a suitable representation \mathcal{R} , i.e., $\mathcal{D} \xrightarrow{\mathbf{T}} \mathcal{R}$;
2. use \mathcal{R} to generate the scanpath, $\mathcal{R} \xrightarrow{\mathbf{T}} \{\mathbf{x}_F(1), \mathbf{x}_F(2), \dots\}$.

Computational modelling has been mainly concerned with the first step: deriving a representation \mathcal{R} (either probabilistic or not). The second step, that is $\mathcal{R} \mapsto \{\mathbf{x}_F(1), \mathbf{x}_F(2), \dots\}$, which actually brings in the question of *how* we look rather than *where*, is seldom taken into account.

In spite of the fact that the most cited work in the field, that by Itti *et al* [55], clearly addressed the *how* issue (gaze shifts as the result of a Winner-Take-All, WTA, sequential selection of most salient locations), most models simply overlook the problem. The computed representation \mathcal{R} is usually evaluated in terms of its capacity for predicting the image regions that will be explored by covert and overt attentional shifts according to some evaluation measure [12]. In other cases, if needed for practical purposes, e.g. for robotic applications, the problem of oculomotor action selection is solved by adopting some deterministic choice procedure that usually relies on selecting the gaze position \mathbf{x} as the argument that maximizes a measure on the given represen-

tation \mathcal{R} (in brief, see [110] for using the $\arg \max_{\mathbf{x}} \mathcal{R}$ operation¹ and [8, 99], for an in-depth discussion).

Yet, another issue arises: the variability of visual scanpaths. When looking at natural movies under a free-viewing or a general-purpose task, the relocation of gaze can be different among observers even though the same locations are taken into account. In practice, there is a small probability that two observers will fixate exactly the same location at exactly the same time. Such variations in individual scanpaths (as regards chosen fixations, spatial scanning order, and fixation duration) still hold when the scene contains semantically rich "objects" (e.g., faces, see Figure 1. Variability is even exhibited by the same subject along different trials on equal stimuli. Further, the consistency in fixation locations between observers decreases with prolonged viewing [31]. This effect is remarkable when free-viewing static images: consistency in fixation locations selected by observers decreases over the course of the first few fixations after stimulus onset [99] and can become idiosyncratic.

The WTA scheme [55, 110], or the selection of the proto-object with the highest attentional weight [111] are deterministic procedures. Even when probabilistic frameworks are used to infer where to look next, the final decision is often taken via the maximum a posteriori (MAP) criterion², which again is an $\arg \max$ operation (e.g., [34, 11, 73, 22]), or variants such as the robust mean (arithmetic mean with maximum value) over candidate positions [2]. As a result, for a chosen visual data input \mathcal{D} the mapping $\mathcal{R} \mapsto \{\mathbf{x}_F(1), \mathbf{x}_F(2), \dots\}$ will always generate the same scanpath across different trials.

There are few notable exceptions to this current state of affairs (see [8] for a discussion). In [58] simple eye-movements patterns, in the vein of [101], are straightforwardly incorporated as a prior of a dynamic Bayesian network to guide the sequence of eye focusing positions on videos. The model presented in [51] embeds at least one parameter suitable to be tuned to obtain different saccade length distributions on static images, although statistics obtained by varying such parameter are still far from those of human data. The model by Keech and Resca [57] mimics phenomenologically the observed eye movement trajectories and where randomness is captured through a Monte Carlo selection of a particular eye movement based on its probability; probabilistic modeling of eye movement data has been also discussed in [91]. However, both models address the specific task of conjunctive visual search and are limited to static scenes. Other exceptions are given, but in the very peculiar field

¹ $\arg \max_x f(x)$ is the mathematical shorthand for "find the value of the argument x that maximizes $f(\cdot)$ "

² Given a posterior distribution $P(X | Y)$ the MAP rule is just about choosing the argument $X = x$ for which $P(X | Y)$ reaches its maximum value (the $\arg \max$) ; thus, if $P(X | Y)$ is a Gaussian distribution, then the $\arg \max$ corresponds to the mode, which for the Gaussian is also the mean value.

Fig. 12 An ensemble of scan paths recorded from different observers while viewing the same image. For visualisation purposes, only five trajectories are shown, different colors coding individual trajectories. If such ensemble is considered to represent the outcome of a stochastic process, the fundamental question that should be answered is: What is the probability $P(\mathbf{x}, t)$ of gazing at location \mathbf{x} at time t ? Images and data are from the Doves dataset [106]



of eye-movements in reading [39]. Other works has addressed the variability issue in the framework of foraging random walks [4, 8, 6, 7, 24, 74].

What we need at least is to bring stochasticity back into the game. As Canosa put it [17]:

Where we choose to look next at any given moment in time is not completely deterministic, yet neither is it completely random

4 Stochastic processes and eye movements

When we randomly sampled a sequence $\{\mathbf{x}(t = 1), \mathbf{x}(t = 2), \mathbf{x}(t = 3), \dots\}$ of gaze shifts from the pdf $P(\mathbf{x})$ (cfr., Eq.8), we were setting up a stochastic process. For example, the *ensemble* of different scan paths on the same viewed image can be conceived as the record of a stochastic process (Figure 12)

Stochastic processes are systems that evolve probabilistically in time or more precisely, systems in which a certain time-dependent random variable $\mathbf{X}(t)$ exists (as to notation, we may sometimes write \mathbf{X}_t instead of $\mathbf{X}(t)$) The variable t usually denotes time and it can be natural or real valued: in the first case, $\mathbf{X}(t)$ is a discrete time stochastic process; in the second case, it is a continuous time stochastic process. We can observe realisations of the process, that is we can measure values

$$\mathbf{X}(t_1) = \mathbf{x}_1, \quad \mathbf{X}(t_2) = \mathbf{x}_2, \quad \mathbf{X}(t_3) = \mathbf{x}_3, \dots,$$

at times t_1, t_2, t_3, \dots . The set \mathcal{S} whose elements are the values of the process is called **state space**.

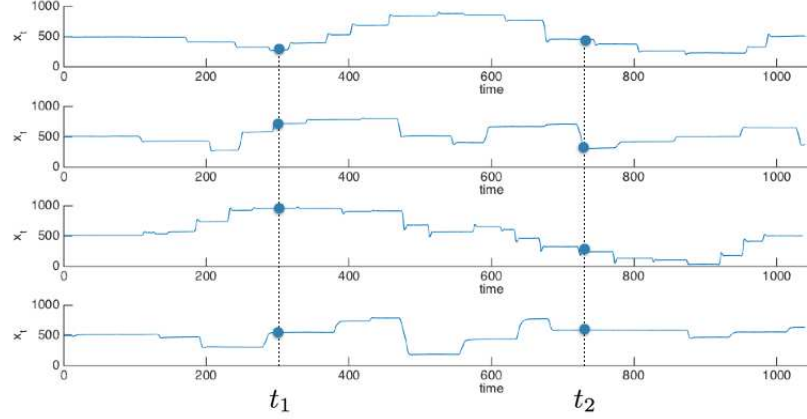


Fig. 13 An ensemble of paths representing a stochastic process. Each path represents the sequence in time of raw x coordinates from different scanpaths recorded on the same picture (cfr. Fig. 12). We can conceive the trajectories of such ensemble as realisations of a stochastic process.

Thus, we can conceive the stochastic process $\mathbf{X}(t)$ as an ensemble of paths as shown in Figure 3 or, more simply, as illustrated in Figure 13: here, for concreteness, we show four series of only the raw x coordinates of different eye-tracked subjects gazing at picture shown in Figure 3. Note that if we fix the time, e.g., $t = t_1$, then $\mathbf{X}(t_1)$ boils down to a RV (vertical values); the same holds if we choose one path \mathbf{x} and we (horizontally) consider the set of values $\mathbf{x}_1, \mathbf{x}_2, \mathbf{x}_3, \dots$, at times t_1, t_2, t_3, \dots .

Use Huang's abbreviation [53]

$$k \leftrightarrow \{\mathbf{x}_k, t_k\}$$

To describe the process completely we need to know the correlations in time, that is the hierarchy of pdfs (but see Table 6, for a discussion of correlation):

$$\begin{aligned} P(1) &: \text{the 1 point pdf} \\ P(1, 2) &: \text{the 2 points pdf} \\ P(1, 2, 3) &: \text{the 3 points pdf} \\ &\dots \end{aligned} \tag{17}$$

up to the n point joint pdf. The n point joint pdf must imply all the lower k point pdfs, $k < n$:

$$P(1, \dots, k) = \int P(1, \dots, n) d\mathbf{x}_{k+1} d\mathbf{x}_{k+2} \dots d\mathbf{x}_n \tag{18}$$

where $P(1, \dots, n)dx_{k+1}dx_{k+2} \dots dx_n$ stands for the joint probability of finding that \mathbf{x} has a certain value

$$\begin{aligned} \mathbf{x}_{k+1} < \mathbf{x} \leq \mathbf{x}_{k+1} + d\mathbf{x}_{k+1} & \text{ at time } t_{k+1} \\ \mathbf{x}_{k+2} < \mathbf{x} \leq \mathbf{x}_{k+2} + d\mathbf{x}_{k+2} & \text{ at time } t_{k+2} \\ & \dots \end{aligned}$$

For instance, referring to Figure 13, we can calculate the joint probability $P(1, 2)dx_1dx_2$ by following the vertical line at t_1 and t_2 and find the fraction of paths for which $\mathbf{x}(t_1) = \mathbf{x}_1$ within tolerance $d\mathbf{x}_1$ and $\mathbf{x}(t_2) = \mathbf{x}_2$ within tolerance $d\mathbf{x}_2$, respectively³

Summing up, the joint probability density function, written explicitly as

$$P(\mathbf{x}_1, t_1; \mathbf{x}_2, t_2; \dots; \mathbf{x}_n, t_n),$$

is all we need to fully characterise the statistical properties of a stochastic process and to calculate the quantities of interest characterising the process (see Table 6).

The **dynamics**, or *evolution* of a stochastic process can be represented through the specification of **transition probabilities**:

$$\begin{aligned} P(2 | 1) & : \text{probability of finding 2, when 1 is given;} \\ P(3 | 1, 2) & : \text{probability of finding 3, when 1 and 2 are given;} \\ P(4 | 1, 2, 3) & : \text{probability of finding 4, when 1, 2 and 3 are given;} \\ & \dots \end{aligned}$$

Transition probabilities for a stochastic process are nothing but the conditional probabilities suitable to predict the future values of $\mathbf{X}(t)$ (i.e., $\mathbf{x}_{k+1}, \mathbf{x}_{k+2}, \dots, \mathbf{x}_{k+l}$, at $t_{k+1}, t_{k+2}, \dots, t_{k+l}$), given the knowledge of the past ($\mathbf{x}_1, \mathbf{x}_2, \dots, \mathbf{x}_k$, at t_1, t_2, \dots, t_k). The conditional pdf explicitly defined in terms of the joint pdf can be written:

$$P(\overbrace{\mathbf{x}_{k+1}, t_{k+1}; \dots; \mathbf{x}_{k+l}, t_{k+l}}^{\text{future}} | \underbrace{\mathbf{x}_1, t_1; \dots; \mathbf{x}_k, t_k}_{\text{past}}) = \frac{P(\mathbf{x}_1, t_1; \dots; \mathbf{x}_{k+l}, t_{k+l})}{P(\mathbf{x}_1, t_1; \dots; \mathbf{x}_k, t_k)}. \quad (25)$$

assuming the time ordering $t_1 < t_2 < \dots < t_k < t_{k+1} < \dots < t_{k+l}$.

By using transition probabilities and the product rule, the following update equations can be written:

$$\begin{aligned} P(1, 2) & = P(2 | 1)P(1) \\ P(1, 2, 3) & = P(3 | 1, 2)P(1, 2) \\ P(1, 2, 3, 4) & = P(4 | 1, 2, 3)P(1, 2, 3) \\ & \dots \end{aligned} \quad (26)$$

³ This gives an intuitive insight into the notion of $P(1, 2)$ as a *density*.

Table 6 How to observe a stochastic process

Consider a series of time signals. The signal fluctuates up and down in a seemingly erratic way. The measurements that are in practice available at one time of a measurable quantity $x(t)$ are the mean and the variance. However, the mean and the variance do not tell a great deal about the underlying dynamics of what is happening. A fundamental question in time series analysis is: to what extent the value of a RV variable measured at one time can be predicted from knowledge of its value measured at some earlier time? Does the signal at t_0 influence what is measured at a later time $t_0 + t$? We are not interested in any specific time instant t_0 but rather in the typical (i.e., the statistical) properties of the fluctuating signal. The amount of dependence, or history in the signal can be characterized by the **autocorrelation function**.

$$C_{xx}(\tau) = \lim_{T \rightarrow \infty} \frac{1}{T} \int_0^T x(t)x(t+\tau)dt \quad (19)$$

This is the time average of a two-time product over an arbitrary large time T , which is then allowed to become infinite. Put simply, is the integral of the product of the time series with the series simply displaced with respect to itself by an amount τ . An autocorrelated time series is predictable, probabilistically, because future values depend on current and past values.

In practice, collected time series are of finite length, say N . Thus, the estimated autocorrelation function is best described as the **sample autocorrelation**

$$c_{xx}(\Delta) = \frac{1}{N} \sum_{n=0}^{N-|\Delta|-1} x(n)x(n+\Delta) \quad (20)$$

Measurements of $C_{xx}(\tau)$ are used to estimate the time-dependence of the changes in the joint probability distribution, where the **lag** is $\tau = t - t_0$. If there is no statistical correlation $C_{xx}(\tau) = 0$. The rate at which $C_{xx}(\tau)$ approaches 0 as τ approaches ∞ is a measure of the **memory** for the stochastic process, which can also be defined in terms of **correlation time**:

$$t_{corr} = \frac{1}{C_{xx}(0)} \int_0^{+\infty} C_{xx}(\tau) d\tau. \quad (21)$$

The autocorrelation function has been defined so far as a **time average** of a signal, but we may also consider the **ensemble average**, in which we repeat the same measurement many times, and compute averages, denoted by symbol $\langle \rangle$. Namely, the correlation function between $x(t)$ at two different times t_1 and t_2 is given by:

$$\langle x(t_1), x(t_2) \rangle = \int_{-\infty}^{+\infty} \int_{-\infty}^{+\infty} x_1 x_2 P(x_1, t_1; x_2, t_2) dx_1 dx_2 \quad (22)$$

. For many systems the ensemble average is equal to the time average, $\langle x \rangle = \int_{-\infty}^{+\infty} x_1 P(x_1, t) dx_1 \approx \lim_{T \rightarrow \infty} \frac{1}{T} \int_0^T x(t) dt = \overline{x(t)}$. Such systems are termed **ergodic**. Ergodic ensembles for which the probability distributions are invariant under time translation and only depend on the relative times $t_2 - t_1$ are **stationary processes**. Thus, if we have a stationary process, it is reasonable to expect that average measurements could be constructed by taking values of the variable x at successive times, and averaging various functions of these.

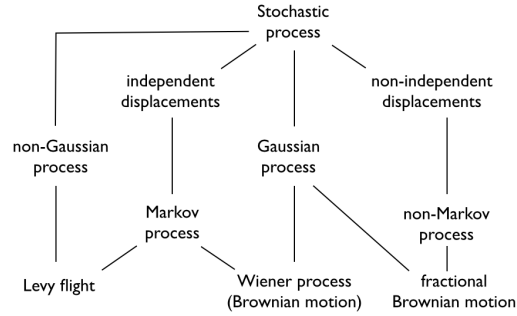
Correlation and memory properties of a stochastic process are typically investigated by analysing the autocorrelation function or the spectral density (**power spectrum**) $S(\omega)$, which describes how the power of a time series is distributed over the different frequencies. These two statistical properties are equivalent for stationary stochastic processes. In this case the *Wiener-Kintchine theorem* holds

$$S(\omega) = \frac{1}{2\pi} \int_{-\infty}^{-\infty} \exp(-i\omega\tau) C_{xx}(\tau) d\tau \quad (23)$$

$$C_{xx}(\tau) = \int_{-\infty}^{-\infty} \exp(i\omega\tau) S(\omega) d\omega \quad (24)$$

It means that one may either directly measure the autocorrelation function of a signal, or the spectrum, and convert back and forth, which by means of the Fast Fourier Transform (FFT) and computer is relatively straightforward. Practically, one can compute the sample power spectral density function using the FFT of the sample autocorrelation, i.e. $s(\omega) = FFT(c_{xx}(\Delta))$, or viceversa by the inverse transform, $c_{xx}(\Delta) = IFFT(s(\omega))$.

Fig. 14 A conceptual map of stochastic processes that are likely to play a role in eye movement modelling and analyses



The transition probabilities must satisfy the normalisation condition $\int P(2 | 1) d\mathbf{x}_2 = 1$. Since $P(2) = \int P(1, 2) d\mathbf{x}_1$ and by using the update eqs. (27), the following evolution (integral) equation holds

$$P(2) = \int \overbrace{P(2 | 1)}^{\text{propagator}} P(1) d\mathbf{x}_1 \quad (27)$$

where $P(2 | 1)$ serves as the *evolution kernel* or *propagator* $P(1 \rightarrow 2)$.

A stochastic process whose joint pdf does not change when shifted in time is called a (strict sense) **stationary process**:

$$P(\mathbf{x}_1, t_1; \mathbf{x}_2, t_2; \dots; \mathbf{x}_n, t_n) = P(\mathbf{x}_1, t_1 + \tau; \mathbf{x}_2, t_2 + \tau; \dots; \mathbf{x}_n, t_n + \tau) \quad (28)$$

$\tau > 0$ being a time shift. Analysis of a stationary process is frequently much simpler than for a similar process that is time-dependent: varying t , all the random variables X_t have the same law; all the moments, if they exist, are constant in time; the distribution of $X(t_1)$ and $X(t_2)$ depends only on the difference $\tau = t_2 - t_1$ (time lag), i.e., $P(\mathbf{x}_1, t_1; \mathbf{x}_2, t_2) = P(\mathbf{x}_1, \mathbf{x}_2; \tau)$.

A conceptual map of main kinds of stochastic processes that we will discuss in the remainder of this Chapter is presented in Figure 14.

5 How to leave the past behind: Markov Processes

The most simple kind of stochastic process is the Purely Random Process in which there are no correlations. From Eq. (27):

$$\begin{aligned} P(1, 2) &= P(1)P(2) & (29) \\ P(1, 2, 3) &= P(1)P(2)P(3) \\ P(1, 2, 3, 4) &= P(1)P(2)P(3)P_1(3) \\ &\dots \end{aligned}$$

One such process can be obtained for example by repeated coin tossing. The complete independence property can be written explicitly as:

$$P(\mathbf{x}_1, t_1; \mathbf{x}_2, t_2; \dots) = \prod_i P(\mathbf{x}_i, t_i), \quad (30)$$

the uppercase greek letter \prod indicates a product of factors, e.g., for $i = 1, 2, 3$, $P(\mathbf{x}_1, t_1; \mathbf{x}_2, t_2; \mathbf{x}_3, t_3) = P(\mathbf{x}_1, t_1)P(\mathbf{x}_2, t_2)P(\mathbf{x}_3, t_3)$.

Equation 30 means that the value of \mathbf{X} at time t is completely independent of its values in the past (or future). A special case occurs when the $P(\mathbf{x}_i, t_i)$ are independent of t , so that the same probability law governs the process at all times. Thus, a completely memoryless stochastic process is composed by a set of **independent and identically distributed** (i.i.d) RVs. Put simply, a series of i.i.d. RVs is a series of samples where individual samples are “independent” of each other and are generated from the same probability distribution (“identically distributed”).

More realistically, we know that most processes in nature, present some correlations between consecutive values (e.g., the direction of the following gaze shift is likely to be positively correlated with the direction of current gaze shift). A step towards a more realistic description consists then of assuming that the next value of each RV in the process depends explicitly on the current one (but not explicitly on any other previous to that). An intuitive example is the *simple random walk* (see Box 7)

If a process has no memory beyond the last transition then it is called a *Markov process* and the transition probability enjoys the property:

$$P(\mathbf{x}_n, t_n | \mathbf{x}_{n-1}, t_{n-1}; \dots; \mathbf{x}_1, t_1) = P(\mathbf{x}_n, t_n | \mathbf{x}_{n-1}, t_{n-1}) \quad (33)$$

with $t_1 < t_2 < \dots < t_n$.

A Markov process is fully determined by the two densities $P(\mathbf{x}_1, t_1)$ and $P(\mathbf{x}_2, t_2 | \mathbf{x}_1, t_1)$; the whole hierarchy can be reconstructed from them. For example, from Equation 27 using the Markov property $P(3 | 1, 2) = P(3 | 2)$:

$$P(1, 2, 3) = P(1)P(2 | 1)P(3 | 2). \quad (34)$$

The algorithm can be continued, and in general the factorization of the joint pdf can be explicitly written,

$$P(\mathbf{x}_n, t_n; \mathbf{x}_{n-1}, t_{n-1}; \dots; \mathbf{x}_1, t_1) = P(\mathbf{x}_1, t_1) \prod_{i=2}^n P(\mathbf{x}_i, t_i | \mathbf{x}_{i-1}, t_{i-1}), \quad (35)$$

with the propagator $P(\mathbf{x}_{i+1}, t_{i+1} | \mathbf{x}_i, t_i)$ carrying the system forward in time, beginning with the initial distribution $P(\mathbf{x}_1, t_1)$.

A well known example of Markov process is the **Wiener-Lévy process** describing the position of a Brownian particle (Fig.15).

Table 7 Random walks

Random walks (RW) are a special kind of stochastic process and can be used, as we will see, to model the dynamics of many complex systems. A particle moving in a field, an animal foraging, and indeed the “wandering” eye can be conceived as examples of random walkers.

Consider t_{corr} the correlation length or memory of the system. If t_{corr} is very large, then a system is said to have a long memory (cfr., Table 6).

In general, RWs exhibit what is called serial correlation, conditional independence for fairly small values of correlation length t_{corr} , and a simple stochastic historical dependence. For instance, a simple additive $1 - D$ random walk has the form:

$$x_t = x_{t-1} + \xi_t, \text{ where } \xi_t \sim P(\xi) \quad (31)$$

In the above formulation, time t proceeds in discrete steps. ξ_t is a RV drawn i.i.d. from a distribution $P(\xi)$, called the *noise* or *fluctuation* distribution. Thus, the differences in sequential observations $x_t - x_{t-1} = \xi_t \sim P(\xi)$ are i.i.d. In other terms, we have here or **independent displacements**.

However, the observations themselves are not independent, since (31) encodes the generative process, or evolution law, $x_{t-1} \rightarrow x_t$ where x_t explicitly depends on x_{t-1} , but not on earlier $x_{t-2}, x_{t-3}, x_{t-4}, \dots$. Thus Eq. (31) represents a Markov process.

Conventionally, fluctuations are normally (Gaussian) distributions with mean μ and variance σ^2 , that is, $\xi \sim \mathcal{N}(\mu, \sigma^2)$, as this makes mathematical analysis considerably simpler. In this case by simply extending to two dimensions ($2 - D$) Eq. 31,

$$\begin{aligned} x_t &= x_{t-1} + \xi_{x,t} \\ y_t &= y_{t-1} + \xi_{y,t}, \end{aligned} \quad (32)$$

the simulation of a simple Brownian RW can be obtained (see Fig. 15).

However, any probability distribution, for instance, a Laplace (exponential tails) or double-Pareto distribution (power-law tails), also works.

The fact that a Markov process is fully determined by $P(1)$ and $P(2 | 1)$ does not mean that such two functions can be chosen arbitrarily, for they must also obey two important identities.

The first one is Equation 27 that in explicit form reads:

$$P(\mathbf{x}_2, t_2) = \int_{\mathbf{x}_1} P(\mathbf{x}_2, t_2 | \mathbf{x}_1, t_1) P(\mathbf{x}_1, t_1) d\mathbf{x}_1. \quad (36)$$

This equation simply constructs the one time probabilities in the future t_2 of t_1 , given the conditional probability $P(\mathbf{x}_2, t_2 | \mathbf{x}_1, t_1)$.

The second property can be obtained by marginalising the joint pdf with respect to \mathbf{x}_2 and using the definition of conditional density under the Markov property:

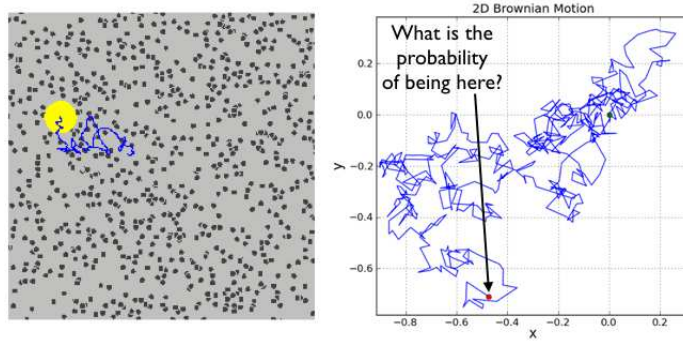
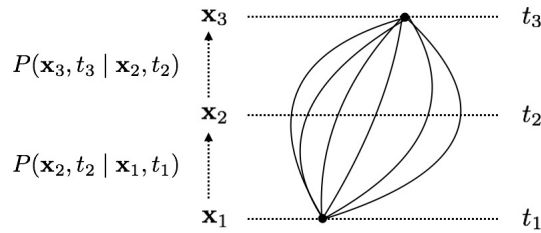


Fig. 15 Motion of a Brownian particle. Left: The physical mechanism of the displacement (in blue): the bigger particle performs a **Brownian motion** (Bm) as a result of the collisions with small particles (figure is not to scale). Right: Sample path of the Bm performed by the bigger particle. Here the fundamental question is: What is the probability of the particle being at location $\mathbf{x} = (x, y)$ at time t ? (cfr. Table 8)

Fig. 16 The Chapman-Kolmogorov equation at work: the probability of transition from the event (\mathbf{x}_1, t_1) to (\mathbf{x}_3, t_3) is broken into a subprocess from (\mathbf{x}_1, t_1) to an intermediate, nuisance event (\mathbf{x}_2, t_2) (which is not observed in practice) and then from (\mathbf{x}_2, t_2) to (\mathbf{x}_3, t_3) , by considering all the paths from \mathbf{x}_1 to \mathbf{x}_3 .



$$P(\mathbf{x}_3, t_3 | \mathbf{x}_1, t_1) = \int_{\mathbf{x}_2} P(\mathbf{x}_3, t_3 | \mathbf{x}_2, t_2)P(\mathbf{x}_2, t_2 | \mathbf{x}_1, t_1)d\mathbf{x}_2, \quad (37)$$

Equation 37 is known as the **Chapman-Kolmogorov Equation**. It is “just” a statement saying that to move from position \mathbf{x}_1 to \mathbf{x}_3 you just need to average out all possible intermediate positions \mathbf{x}_2 or, more precisely, by marginalization over the nuisance variable \mathbf{x}_2 .

Such equation is a consistency equation for the conditional probabilities of a Markov process and the starting point for deriving the equations of motion for Markov processes. Aside from providing a consistency check, the real importance of the C-K equation is that it enables us to build up the conditional probability densities over the “long” time interval $[t_1, t_3]$ from those over the “short” intervals $[t_1, t_2]$ and $[t_2, t_3]$.

The C-K Equation is a rather complex nonlinear functional equation relating all conditional probabilities $P(\mathbf{x}_i, t_i | \mathbf{x}_j, t_j)$ to each other. Its solution would give us a complete description of any Markov process, but unfortu-

nately, no general solution to this equation is known: in other terms, it expresses the Markov character of the process, but containing no information about any particular Markov process.

The idea of forgetting the past so to use the present state for determining the next one might seem an oversimplified assumption when dealing, for instance, with eye movements performed by an observer engaged in some overt attention task. However, this conclusion may not be so obvious as discussed by Horowitz and Wolfe [52].

5.1 Case study: the Horowitz and Wolfe hypothesis of amnesic visual search

Serial and parallel theories of visual search have in common the memory-driven assumption that efficient search is based on accumulating information about the contents of the scene over the course of the trial.

Horowitz and Wolfe in their seminal Nature paper [52] tested the hypothesis whether visual search relies on memory-driven mechanisms. They designed their stimuli so that, during a trial, the scene would be constantly changing, yet the meaning of the scene (as defined by the required response) would remain constant. They asked human observers to search for a letter “T” among letters “L”. This search demands visual attention and normally proceeds at a rate of 20 – 30 milliseconds per item. In the critical condition, they randomly relocated all letters every 111 milliseconds. This made it impossible for the subjects to keep track of the progress of the search. Nevertheless, the efficiency of the search was unchanged.

On the basis of achieved results they proposed that visual search processes are “amnesic”: they act on neural representations that are continually rewritten and have no permanent existence beyond the time span of visual persistence.

In other terms, the visual system does not accumulate information about object identity over time during a search episode. Instead, the visual system seems to exist in a sort of eternal present. Observers are remarkably oblivious to dramatic scene changes when the moment of change is obscured by a brief flicker or an intervening object.

Interestingly enough, they claim that an amnesic visual system may be a handicap only in the laboratory. The structure of the world makes it unnecessary to build fully elaborated visual representations in the head. Amnesia may be an efficient strategy for a visual system operating in the real world.

Table 8 The hall of fame of Markov processes

The most famous Markov process is the Wiener-Lévy process describing the position of a Brownian particle. Figure 15 shows an example of the 2D motion of one such particle. A probabilistic description of the random walk of the particle must answer the question: What is the probability $P(\mathbf{x}, t)$ of the particle being at location $\mathbf{x} = (x, y)$ at time t ?

In the 1D case, the probability $P(x, t)$ and its evolution law are defined for $-\infty < x < \infty$, $t > 0$ by the densities

$$P(x, t) = \frac{1}{\sqrt{4\pi Dt}} \exp\left(-\frac{x^2}{4Dt}\right), \quad (38)$$

$$P(x_2, t_2 | x_1, t_1) = \frac{1}{\sqrt{4\pi D(t_2 - t_1)}} \exp\left(-\frac{(x_2 - x_1)^2}{4D(t_2 - t_1)}\right). \quad (39)$$

that satisfy the Chapman-Kolmogorov equation. Here D denotes a **diffusion coefficient**.

5.2 Stationary Markov processes and Markov chains

Recall that for stationary Markov processes the transition probability $P(\mathbf{x}_2, t_2 | \mathbf{x}_1, t_1)$ does not depend on two times but only on the time interval. For this case one can introduce the special notation

$$P(\mathbf{x}_2, t_2 | \mathbf{x}_1, t_1) = T_\tau(\mathbf{x}_2 | \mathbf{x}_1) \text{ with } \tau = t_2 - t_1. \quad (40)$$

The Chapman-Kolmogorov equation then becomes

$$T_{\tau+\tau'}(\mathbf{x}_3 | \mathbf{x}_1) = \int_{\mathbf{x}_2} T_{\tau'}(\mathbf{x}_3 | \mathbf{x}_2) T_\tau(\mathbf{x}_2 | \mathbf{x}_1) d\mathbf{x}_2. \quad (41)$$

If one reads the integral as the product of two matrices or integral kernels, then

$$T_{\tau+\tau'} = T_{\tau'} T_\tau \quad (\tau, \tau' > 0) \quad (42)$$

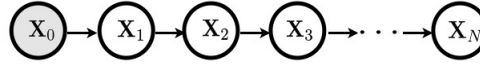
A simple but important class of stationary Markov processes are the **Markov chains** defined by the following properties:

1. the state space of \mathbf{x} is a *discrete set of states*;
2. the *time variable is discrete* and takes only integer values;

In this case the dynamics can be represented as the PGM in Figure 17. The PGM shows that the joint distribution for a sequence of observations $P(\mathbf{x}_0, \mathbf{x}_1, \mathbf{x}_2, \dots, \mathbf{x}_N)$ can be written as the product:

$$P(\mathbf{x}_1) P(\mathbf{x}_2 | \mathbf{x}_1) \cdots P(\mathbf{x}_N | \mathbf{x}_{N-1}) = P(\mathbf{x}_1) \prod_{t=2}^N P(\mathbf{x}_t | \mathbf{x}_{t-1}) \quad (43)$$

Fig. 17 The PGM of a Markov chain: given the prior or initial condition $P(\mathbf{x}_1)$, the behaviour of the system is determined by the conditional probability $P(\mathbf{x}_t | \mathbf{x}_{t-1})$



This is also known as an **observable Markov process**.

A **finite Markov chain** is one whose range consists of a finite number of N states. In this case the first probability distribution is an N component vector. The transition probability $T_\tau(\mathbf{x}_2 | \mathbf{x}_1)$ is an $N \times N$ matrix

Thus, the C-K equation, by using the form in Eq. 44, leads to the matrix equation

$$T_\tau = (T_1)^\tau \quad (44)$$

Hence the study of finite Markov chains amounts to investigating the powers and the properties of the $N \times N$ transition matrix whose elements are nonnegative and each column adds up to unity. One seminal application of Markov chains to scanpaths has been provided by Ellis and Stark [35].

5.2.1 Case study: modeling gaze shifts as observable finite Markov chains

Ellis and Stark pioneered the use of Markov analysis for characterizing scanpaths [35] in an attempt to go beyond visual inspection of the eye movement traces and application of a subjective test for similarity of such traces. In particular, they challenged the assumption of what they defined “apparent randomness”, that many studies at the time were supporting in terms of either simple random or stratified random sampling [35]. To this end (see Figure 18), they defined regions of interest (ROI) defined on the viewed picture, each ROI denoting a *state* into which the fixations can be located. By postulating that the transitions from one state to another have certain probabilities, they effectively described the generating process for these sequences of fixations as Markov processes. This way, they were able to estimate the marginal probabilities of viewing a point of interest i , i.e., $P(X = s_i)$, and the conditional probability of viewing point of interest j given previous viewing of point of interest i , i.e., $T(X = s_j | X = s_i)$, where s_i, s_j are states in the state-space S (see Figure 18).

By comparing expected frequency of transitions according to random sampling models with observed transition frequencies, they were able to assess the statistically significant differences occurred (subject-by-subject basis with a chi-square goodness-of-fit test on the entire distribution of observed and expected transitions). Thus, they concluded that “there is evidence that something other than stratified random sampling is taking place during the scan-



Fig. 18 Markov analysis of eye movements made by a subject viewing for the first time a drawing adapted from the Swiss artist Klee (left). Center: ROIs superimposed on the drawing, defining the states of the Markov chain: $S = \{s_1 = \text{“left eye”}, s_2 = \text{“right eye”}, s_3 = \text{“nose”}, s_4 = \text{“mouth”}, s_5 = \text{“hand”}, s_6 = \text{“neck”}\}$. Right: saccades represented as state transitions in the state-space. Modified after [44, 35]

ning” [35]. In a further study [44], examples have been provided for exploiting the observable Markov chain as a generative machine apt to sample simulated scanpaths, once the transition matrix has been estimated / learned from data.

5.3 Levels of representation of the dynamics of a stochastic process

If we carefully inspect scan paths such as those shown in Figures 1 and 12 it is intuitive to recognise the signature of some kind of random walk. In this perspective it makes sense to re-formulate the fundamental question raised for simple Bm as “What is the probability $P(\mathbf{x}, t)$ of gazing at location \mathbf{x} at time t ?”

There are three different levels to represent and deal with the properties of stochastic processes, and in particular RWs: microscopic, mesoscopic and macroscopic.

The C-K equation discussed so far can be regarded as a **mesoscopic** balance equation for the transition probabilities defining the evolution of the random variable $X(t)$.

The **microscopic description** of a system consists in modeling the system with evolution equations or **differential equations**, see Table 9, that directly describe the **fine-grained dynamics**, that is individual trajectories: e.g., the path of a Brownian particle or the scan path of an eye-tracked observer. A simple form of such equations is the following:

$$\overbrace{\frac{dx}{dt}}^{\text{state-space rate of change}} = \overbrace{a(x, t)}^{\text{deterministic comp.}} + \overbrace{b(x, t)\xi(t)}^{\text{stochastic comp.}}, \quad (45)$$

which we call the **Langevin equation**, in analogy with the well known equation that in statistical physics describes the time evolution of the velocity of a Brownian particle. In Eq. 45 the drift term $a(x, t)$ represents the deterministic component of the process; the diffusive component $b(x, t)\xi(t)$ is the stochastic component, $\xi(t)$ being the “noise” sampled from some probability density, i.e. $\xi(t) \sim P(\xi)$ usually a zero-mean Normal distribution.

Equation (45) is a **stochastic differential equation** (SDE), which in a more formal way can be written in the Ito form of Eq.52 as detailed in Table 10

Table 9 Dynamical systems and differential equations

A system that changes with time is called a **dynamical system**. A dynamical system consists of a space of states and entails a law of motion between states, or a **dynamical law** The deterministic component of Langevin Eq. 45

$$\frac{dx(t)}{dt} = a(x(t), t) \quad (46)$$

is one such law, the variable $x(t)$ being the variable that, moment to moment, takes values in the state space of positions. Equation 46 is a **differential equation** describing the rate of change of state-space variable x .

In simple terms, a dynamical law is a rule that tells us the next state given the current state. This can be more readily appreciated if we recall the definition of derivative given in Table 1, but avoid to apply the shrinking operation ($\lim_{\Delta t \rightarrow 0}$), i.e. we approximate the derivative as a discrete difference $\frac{dx(t)}{dt} \approx \frac{x(t+\Delta t) - x(t)}{\Delta t}$. By assuming for simplicity a unit time step, i.e., $\Delta t = 1$ and substituting in Eq. 46

$$\overbrace{x(t+1)}^{\text{next state}} = \overbrace{x(t)}^{\text{current state}} + a(x(t), t) \quad (47)$$

Eq. 47 is the discrete-time version of the differential equation 46, namely a finite-difference equation. The model in discrete time emphasises the predictive properties of the law: indeed, with the scientific method we seek to make predictions about phenomena that are subject to change. Caveat: we should always be cautious about how predictable the world is, even in classical physics. Certainly, predicting the future requires a perfect knowledge of the dynamical laws governing the world but at the same time entails the ability to know the initial conditions with almost perfect precision. However, perfect predictability is not achievable, simply because we are limited in our resolving power. There are cases in which the tiniest differences in the initial conditions (the starting state), leads to large eventual differences in outcomes. This phenomenon is called *chaos*.

The law formalised in Eqs. 46 or 47 are deterministic. In stark contrast, the Langevin equation (45) “corrupts” the deterministic law of motion with the “noise” introduced by the RV $\xi(t)$, thus the eventual outcome is not deterministic but stochastic (though it may be predictable in probability). Langevin equation is but one example of **stochastic differential equation** (SDE).

Concretely, the construction of a trajectory (a solution) can be performed by refining the intuitive discretisation approach presented in Table 9. Eq. 45 is discretised as in Eq. 54 by executing a sequence of drift and diffusion steps as illustrated in Figure 20.

In continuous time a 2-dimensional random motion of a point, with stochastic position $\mathbf{r}(t)$, under the influence of an external force field can be described by the Langevin stochastic equation [94]

$$d\mathbf{x}(t) = \mathbf{A}(\mathbf{x}, t)dt + \mathbf{B}(\mathbf{x}, t)\boldsymbol{\xi}dt. \quad (48)$$

As in the one-dimensional case, the trajectory of \mathbf{x} is determined by a deterministic part \mathbf{A} , the drift, and a stochastic part $\mathbf{B}(\mathbf{x}, t)\boldsymbol{\xi}dt$, where $\boldsymbol{\xi}$ is a random vector and \mathbf{B} is a diffusion factor.

However, to gain a more general picture of the process, we might be interested in the **coarse-grained dynamics**: namely, how the pdf of the system evolves in the large scale limit. This corresponds to the *macroscopic* level of description. There are two possible macroscopic limits from mesoscopic equations: the macroscopic limit in time or in space. When we consider the macroscopic limit in time of the C-K equation, we obtain the **Master equation**; when we consider the macroscopic limit both in time and in the state space of the C-K equation, we obtain the **Fokker-Planck** (F-P) equation.

The Fokker-Planck equation for diffusive (Markovian) processes is the following:

$$\frac{\partial P(x, t)}{\partial t} = -\frac{\partial}{\partial x}[a(x, t)P(x, t)] + \frac{1}{2}\frac{\partial^2}{\partial x^2}[b(x, t)^2P(x, t)] \quad (49)$$

The symbols $\frac{\partial}{\partial t}$, $\frac{\partial}{\partial x}$ and $\frac{\partial^2}{\partial x^2} = \frac{\partial}{\partial x}(\frac{\partial}{\partial x})$ denote *partial derivatives* of first and second-order, respectively.⁴

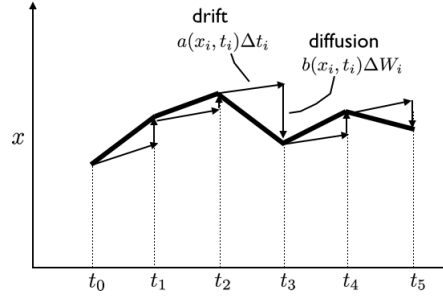
Equation (49) is a **partial differential equation** (PDE) defining the “law of motion” of the density $P(x, t)$ in probability space.

There is a precise link between the microscopic description provided by the Langevin equation and the macroscopic description addressed by the F-P equation, which is established via $a(x, t)$ and $b(x, t)$. The term $a(x, t)$ represents a **drift** which is related to the average deviation of the process

$$a(x, t) = \lim_{\Delta t \rightarrow 0} \frac{\langle \Delta x \rangle}{\Delta t}. \quad (50)$$

⁴ If we have a function of more than one variable, e.g., $f(x, y, z, \dots)$, we can calculate the derivative with respect to one of those variables, with the others kept fixed. Thus, if we want to compute $\frac{\partial f(x, y, z, \dots)}{\partial x}$, we define the increment $\Delta f = f([x + \Delta x], y, z, \dots) - f(x, y, z, \dots)$ and we construct the partial derivative as in the simple derivative case as $\frac{\partial f(x, y, z, \dots)}{\partial x} = \lim_{\Delta x \rightarrow 0} \frac{\Delta f}{\Delta x}$. By the same method we can obtain the partial derivative with respect to any of the other variables.

Fig. 19 The Cauchy-Euler procedure for constructing an approximate solution of the Langevin SDE in the Ito form (cfr. Table 10)



over a small time interval Δt . The term $b^2(x, t)$ represents a **diffusion** term, which is related to the mean square deviation of the process:

$$b^2(x, t) = \lim_{\Delta t \rightarrow 0} \frac{\langle (\Delta x)^2 \rangle}{\Delta t}. \quad (51)$$

At the macroscopic level, by knowing the evolution of $P(x, t)$ in time, one can obtain statistical ‘observables’ as the moments, correlations, etc. These obviously lack some microscopic details from the underlying stochastic process, which for some specific purposes may be important.

We will turn now to the fundamental example of the Wiener process to make clear the connections between the macroscopic and microscopic levels of description.

5.3.1 Example: the Wiener process

Recall again the most famous Markov process: the Wiener process describing Brownian motion (cfr., Box 8). The SDE defining the motion of a particle undergoing (1-D) Brownian motion can be obtained by setting to zero the drift component $a(x, t)$ and letting $b(x, t) = \sqrt{2D}$, where D is the diffusion coefficient; thus:

$$dx = \sqrt{2D}dW(t) \quad (57)$$

By using Eq. (54) (cfr Table 10), the discretized version of the Wiener process (57) over a small but finite time interval $\Delta t = T/N$, N being the discrete number of integration steps can be written as

$$x_{i+1} = x_i + \sqrt{2D}\Delta W_i = x_i + \sqrt{2D\Delta t}\xi_i \quad (58)$$

with ξ sampled from a zero-mean Gaussian distribution of unit variance $\mathcal{N}(0, 1)$

Equation 58 shows that the system describes a refined version of the simple additive random walk. Once again, it is worth noting that the structure in Eq. (58) is different from a traditional i.i.d process: since $\xi(t)$ are sampled

Table 10 Ito Stochastic Differential Equation: Definition

The Langevin equation written in the form (45) poses some formal problems. Since $\xi(t)$ is noise it consists of a set of points that in some cases can be even uncorrelated. In consequence $\xi(t)$ is often non-differentiable. Thus $x(t)$ should be non-differentiable too, so that the left hand side of (45) is incoherent from this point of view. To overcome this problem, the 1 - D Langevin equation is more formally presented in the mathematically sound form:

$$dx(t) = a(x(t), t)dt + b(x(t), t)\xi(t)dt = a(x(t), t)dt + b(x(t), t)dW(t) \quad (52)$$

with $W(t) = \int_0^t \xi(t')dt'$, so that the integration of the stochastic component $\int b(x, t)dW(t)$ can be performed according to the rules of stochastic calculus (in the Itô or Stratonovich approach []). Throughout this chapter we shall use with a certain liberality both forms (45) and (52) at our convenience. Thus, a stochastic quantity $x(t)$ obeys an Ito SDE written as in (52), if for all t and t_0 ,

$$x(t) = x(t_0) + \int_{t_0}^t a(x(t'), t')dt' + \int_{t_0}^t b(x(t'), t')dW(t') \quad (53)$$

A discretised version of the SDE can be obtained by taking a mesh of points t_i (Fig.??)

$$t_0 < t_1 < t_2 < \dots < t_{n-1} < t_n = t$$

and writing the equation as

$$x_{i+1} = x_i + a(x_i, t_i)\Delta t_i + b(x_i, t_i)\Delta W_i \quad (54)$$

Here, $x_i = x(t_i)$ and

$$\Delta t_i = t_{i+1} - t_i, \quad (55)$$

$$\Delta W_i = W(t_{i+1}) - W(t_i) \propto \sqrt{\Delta t_i}\xi_i. \quad (56)$$

The approximate procedure for solving the equation is to calculate x_{i+1} from the knowledge of x_i by adding a deterministic term $a(x_i, t_i)\Delta t_i$ and a stochastic term $b(x_i, t_i)\Delta W_i$, which contains the element ΔW_i , namely the increment of the Wiener process. The solution is then formally constructed by letting the mesh size go to zero. The method of constructing a solution outlined above is called the Cauchy-Euler method, and can be used to generate simulations. By construction the time development of $x(t)$ for $t > t_0$ is independent of $x(t)$ for $t > t_0$ provided $x(t_0)$ is known. Hence, $x(t)$ is a Markov process.

i.i.d, it is the the differences in sequential observations that are i.i.d, namely, $x_{i+1} - x_i = \Delta x_i$, rather than the observations themselves. In fact, if we compute the auto-correlation function of the $\{x(t)\}$ time series, it exhibits a slower decay —differently from the white noise process—, which shows how this simple random walk exhibits memory (Fig. 20).

Now, assume to simulate the Brownian motion of a large number of particles, say 10^5 . We can obtain this result by running in parallel 10^5 random walks each walk being obtained by iterating Eq.(58). Figure 21 (top) shows

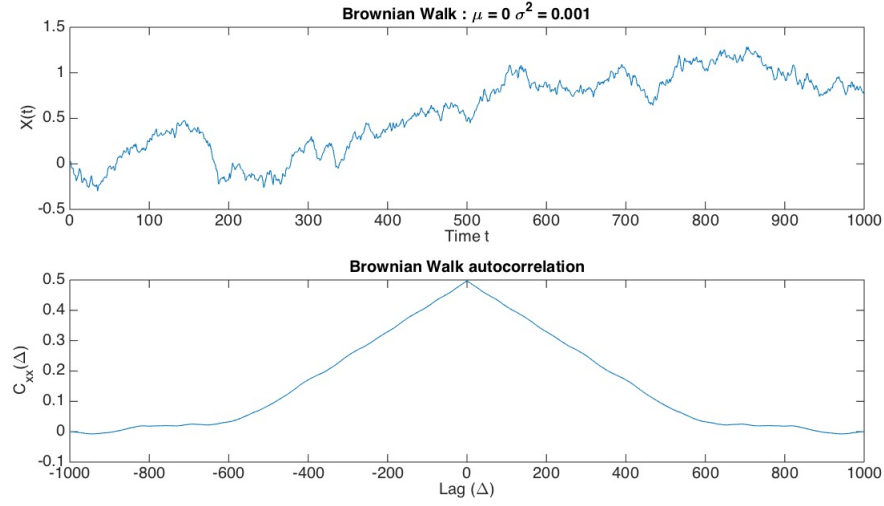


Fig. 20 One dimensional Brownian motion. Top: the random walk process; bottom: the autocorrelation of the process. (cfr. Table 6)

an example of 20 such trajectories. In probabilistic terms each trajectory is then realisation, a sample of the stochastic process $\{X(t)\}$.

We may be interested in gaining some statistical insight of the collective behaviour of all such random walkers. This can be obtained by considering the the dynamics of the pdf $P(x, t)$ describing the probability of finding a particle at position x at time t . Empirically, we can estimate $P(x, t)$ at any time t by computing the density of particles occurring within a certain bin $(x - \delta x, x + \delta x)$, that is by computing the histogram $h(x, t)$ and normalising it with respect to the total number of particles. This procedure is shown in the bottom of Figure 21: the empirical pdf has a nice bell shape, i.e. it is a Normal distribution, which spreads as time increases.

This insight can be given a formal justification by resorting to the macroscopic level of description of process dynamics as provided by F-P equation (49). By setting again $a(x, t) = 0$ and $b(x, t) = \sqrt{2D}$:

$$\frac{\partial P(x, t)}{\partial t} = D \frac{\partial^2 P(x, t)}{\partial x^2} \quad (59)$$

This is the well-known **heat** or **diffusion equation**. Thus, the pdf $P(x, t)$ of finding a particle at position x at time t evolves in time according to the diffusion equation when the underlying microscopic dynamics is such that the particle position corresponds to a Wiener process.

The solution to the heat equation (59) is the time-dependent Gaussian pdf:

$$P(x, t) = \frac{1}{\sqrt{4\pi Dt}} \exp\left(-\frac{x^2}{4Dt}\right), \quad (60)$$

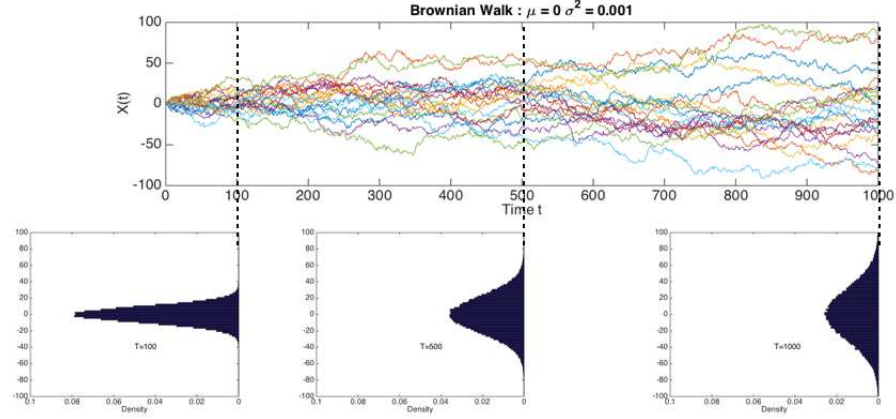


Fig. 21 Top: The simulation of individual trajectories of 10^5 random walkers: only 20 are shown for visualisation purposes. Bottom: The distributions (histograms) of the walkers, after $T = 100$, $T = 500$ and $T = 1000$ time steps. The distribution initially concentrated at a point takes later the Gaussian form, whose width grows in time as $t^{1/2}$. This kind of diffusion is called the *normal diffusion*.

By comparing to the pdf in Eq. (60) introduced in our preliminary definition of the Wiener process, we can set the following correspondences:

$$\sigma^2 = 2Dt = b^2t \approx \langle x^2 \rangle \quad (61)$$

In other terms for Bm, the second moment of the walk and thus the spread of the Gaussian grows linearly with time, as it can be intuitively appreciated from Figure 21.

More precisely, define the **Mean Square Displacement** (MSD) of a walk that starts at position x_0 at time t_0 :

$$MSD = \langle |x - x_0|^2 \rangle \quad (62)$$

that is the square of the displacement in the direction of the x -axis “that a particle experiences on the average” [33], where x_0 denotes the initial position. In the case of Brownian motion (Bm), Einstein [33] was the first to show that:

$$MSD = 2Dt \quad (63)$$

Note that $\langle |x - x_0|^2 \rangle = \langle x^2 \rangle + x_0^2 - 2x_0 \langle x \rangle$, thus when the initial position is at $x_0 = 0$, $MSD = \langle x^2 \rangle \propto t$.

Equation 63 is sometimes written more generally in terms of the **Hurst exponent** H

$$MSD = kt^{2H} \quad (64)$$

with $H = \frac{1}{2}$ for Bm. This is useful for characterising different kinds of diffusions (like hyperdiffusion or subdiffusion)

Table 11 The Hurst exponent: the Swiss army knife of diffusion processes (without SDEs)

The Hurst exponent, H , is a spy on signal correlation behavior and allows the detection of the long-range dependences. In general, properties of Gaussian diffusion may be expressed in terms of the MSD of x and its relation to time:

$$MSD = \langle |x(t) - x(0)|^2 \rangle = kt^{2H} \quad (65)$$

When $H = 0.5$, MSD is linear in time:

$$MSD = kt, \quad (66)$$

which exemplifies the ordinary condition of Bm, the derivative of Bm being additive white Gaussian noise. When $H > 0.5$, increments are positively correlated, i.e. the random walk shows the tendency to continue to move in the current direction. This behavior is called **persistence**. In this case, MSD increases nonlinearly with respect to time, indicative of **hyperdiffusion**. In particular, for $H = 1$,

$$MSD = kt^2, \quad (67)$$

i.e., diffusion follows correlated **fractional Brownian motion** (fBm), whose derivative is fractional Gaussian noise.

In the case $H < 0.5$, the random walk generates negatively correlated increments and is **anti-persistent**

It is important to note that for $H \neq 0.5$, the increments are not independent, thus the fBm is a Gaussian process but it is not a Markov process.

By contrast, the divergence of $\langle x^2 \rangle \rightarrow \infty$ indicates non-Gaussian diffusion:

Interesting work has been reported in the recent literature on the use of the H exponent to analyse eye movements, e.g. by Engbert and colleagues on random walk analysis of fixational eye movements [36]. For such purposes the scaling exponent H can be estimated as follows [36]. Consider a time series of gaze positions of length N , $\mathbf{x}_1, \dots, \mathbf{x}_N$. Define the displacement estimator

$$\overline{\delta^2(\Delta_m)} = \frac{1}{N-m} \sum_{i=1}^{N-m} \|\mathbf{x}_{i+m} - \mathbf{x}_i\|^2, \quad (68)$$

namely the **time averaged MSD**. By recalling that $MSD \approx t^{2H}$, Hurst exponent H can be obtained by calculating the slope in a log – log plot of $\overline{\delta^2(\Delta_m)}$ versus lag $\Delta_m = mT_0$, where T_0 (ms) is the sampling time interval.

More recently, Engbert has proposed more sophisticated estimation framework based on the Bayesian approach [65].

As a last, but important remark, the equivalence

$$\overline{\delta^2(\Delta)} \approx \langle x(\Delta)^2 \rangle \quad (69)$$

holds when the process is **ergodic**, where ensemble averages and long-time averages are equivalent in the limit of long measurement times.

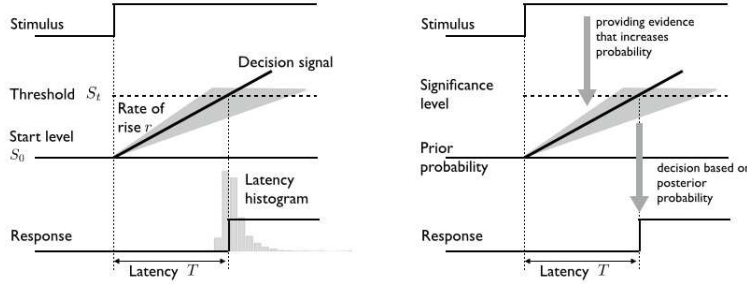


Fig. 22 The LATER model [18]. Left: the original model. Right: LATER as an ideal Bayesian decision-maker

5.3.2 Case study: from random walks to saccade latency

A saccade represents the output of a decision, a choice of where to look, and reaction time, or latency, can be regarded as an experimental “window” into decision processes. In experimental paradigms, reaction time varies between one trial and the next, despite standardized experimental conditions. Furthermore, distribution of reaction times is typically skewed, with a tail towards long reaction times. However, if we take the reciprocal of the latencies and plot these in a similar fashion, the resulting distribution appears Gaussian. A Gaussian or normal distribution of reciprocal latencies implies that these reciprocals have equal variability around a mean value. Such a distribution can then be explained by a very simple and elegant model, the LATER model (“Linear Approach to Threshold with Ergodic Rate” [18]) is one of the simplest, and yet one of the most powerful models of reaction time distributions in decision tasks: it is assumed that some decision signal is accumulated over time at a constant rate until a threshold is reached, at which point a response is triggered (Fig. 22 , right). Crucially, the rate at which such decision signal accumulates is normally distributed across trials. In mathematical terms, the model is easily specified. If the response is triggered when the evidence - starting from a resting level S_0 - reaches a threshold level S_T , and evidence accumulates at a constant rate r which, across trials, follows a normal distribution, $\mathcal{N}(\mu_r, \sigma_r^2)$, the response latency T is determined by:

$$T = \frac{S_T - S_0}{r}. \quad (70)$$

If one further assumes that both S_0 and S_T are relatively constant across trials, then the distribution of the times is the reciprocal of a normal distribution:

$$\frac{1}{T} = \mathcal{N}\left(\frac{\mu_r}{S_T - S_0}, \left(\frac{\mu_r}{S_T - S_0}\right)^2\right), \quad (71)$$

which Carpenter terms the Recinormal distribution.

We can thus consider the function $S(t)$, namely the evidence accumulated at time t starting from prior level $S(0) = S_0$ in the process of reaching the threshold S_T . It can be shown that the average accumulation of evidence $\langle S(t) \rangle$ with mean rate r is described by a normal distribution centered at a mean $S_0 + rt$ having variance at time t equal to $\sigma_r^2 t^2$ [82]. This probabilistic behavior at the macroscopic level corresponds to a microscopic behavior of the random walker $S(t)$ described by a Langevin-type SDE of drift r and diffusion coefficient $\sigma_r \sqrt{2t}$:

$$dS(t) = rdt + \sigma_r \sqrt{2t} dW(t), \quad (72)$$

where $W(t)$ is the standard Wiener process with linear drift. Thus LATER can be considered a non-linear version of the Drift Diffusion Model [86] of decision making.

One implication of all this is that the large random variation observed in latencies is not the result of noise at the input, as has commonly been supposed, but represents a gratuitous, “deliberate” randomising device whose purpose is presumably to prevent the generation of undesirably stereotyped behaviour - a roulette-wheel within the brain, that one may or may not care to think of as the basis for the sense of free will.

5.4 Walking on the safe side: the Central Limit Theorem

Recall from Box 8 that the probability $P(\mathbf{x}, t)$ of a Brownian particle being at location \mathbf{x} at time t is a Gaussian distribution. Also, by resorting to a macroscopic description we have seen that the solution of the diffusion equation for a large number of Brownian particles is the Gaussian distribution.

The Gaussian or Normal distribution correctly describes an amazing variety of phenomena. The bell-shaped curve appears in nature ubiquitously due to the wide applicability of the **Central Limit Theorem (CLT)**, which states that:

The distribution $P(S_n)$ for the sum S_n of a large number n of

1. *statistically independent* and
2. *identically distributed* (i.i.d) RVs that
3. have a *finite variance*,

converges to a Gaussian.

The CLT theorem provides a thorough intuition of the Gaussian nature of a Brownian random walk. Consider the discretisation of the Wiener process as in Equation 58 and set for simplicity $D = 1/2$: it is easy to see that by repeated substitution and by assuming the initial condition $x_0 = 0$:

$$\begin{aligned}
x_{i+1} &= x_i + \Delta W_i \\
&= x_{i-1} + \Delta W_{i-1} + \Delta W_i \\
&= \dots \\
&= \sum_{i=1} \Delta W_i
\end{aligned} \tag{73}$$

Note that by definition of Bm the Wiener increment $x_{i+1} - x_i = \Delta W_i = \xi_i \Delta t_i$ is independently sampled at each discrete step with $\xi_i \sim \mathcal{N}(0, 1)$. Thus, the last equation tells that for any t the position of the walker can be obtained as the sum of a number of i.i.d displacements. Due to the CLT, for a large number of steps, the probability $P(x_n)$ converges to a Gaussian PDF.

As stated previously, the scaling law $\langle x(t)^2 \rangle \propto t$ is characteristic of the diffusion equation, but it also arises asymptotically in many other cases. This is not a coincidence but a direct consequence of the CLT. If a trajectory consists of a set of **independent displacements** then the total distance covered (this is, the sum of all these displacements) tends to a Gaussian distribution of the type $\sim \exp(-\frac{x^2}{\sigma})$ with a parameter σ which, according to the CLT, is proportional to the number of these displacements (and, in consequence, proportional to time). Then the scaling $\langle x(t)^2 \rangle \propto t$ arises immediately from $\langle x(t)^2 \rangle = \sigma$ for a Gaussian distribution with zero mean. If the three conditions required by the CLT are fulfilled, then the MSD will behave at large times like $\langle x(t)^2 \rangle \propto t$ (no matter how complicated the motion pattern is) in the limit $t \rightarrow \infty$.

Table 12 The Gaussian bell tolls for thee: The Central Limit Theorem

Consider n i.i.d RVs X_1, X_2, \dots, X_n , that without loss of generality have zero means $E[X_i] = 0$ and finite variances $E[X_i^2] = s_i^2$. Consider then the RV which is the sum

$$S_n = X_1 + X_2 + \dots + X_n \tag{74}$$

with

$$\sigma_n^2 = \frac{s_1^2 + s_2^2 + \dots + s_n^2}{n} \tag{75}$$

Then the CLT states that as n approaches infinity

$$S_n \sim \frac{1}{\sqrt{2\pi\sigma_n}} \exp\left(-\frac{S_n^2}{2\sigma_n^2}\right), \tag{76}$$

that is S_n converges to a stochastic process with Gaussian distribution. A Formal proof of the CLT is given in probability text such as Feller's [38].

An implication of the CLT is that if the sum S_n tends to a Gaussian variable, so does the average value $\frac{X_1 + X_2 + \dots + X_n}{n}$. In consequence, any problem where the final output results from the average over a set of identical and independent variables leads to a Gaussian PDF.

6 Walking on the wild side: eye movements beyond the CLT

In spite of the nice behaviour of RWs patrolled by the CLT, when dealing with eye movements most interesting cases happen when the CLT is violated:

- (i) Violation of independency: Long-range correlations are present, so once the random walker decides moving in one direction it keeps on doing the same for a long time (this will lead to superdiffusion) or, alternatively, once it stops it remains resting for an arbitrarily long time (then subdiffusion will emerge)
- (ii) Violation of identity: motion consists of non-identical displacements that become gradually shorter (subdiffusion) or longer (superdiffusion) probably because of external constraints.
- (iii) Violation of moment finiteness: The displacements forming the trajectory can be fitted to a PDF with non-finite mean or variance, so as a result arbitrarily large displacements are likely with a certain frequency (long tail distributions)

When one of the three conditions is violated then the process is said to exhibit **anomalous diffusion**. A simple way to define anomalous diffusion or an anomalous random walk is when $\langle x(t)^2 \rangle$ does not increase linearly with time. In these cases the corresponding MSD shows a power-law behaviour

$$MSD = kt^\gamma, \quad (77)$$

with $\gamma \neq 1$

6.1 A first violation: *i.i.d* denied

One way to anomalous diffusion is by introducing “memory” effects in the process. This gives rise to **long-range** power-law autocorrelations in the underlying noise that drives the random walk. Long-range memory effects violate the condition of independent random variables.

One intuitive example is the self-avoiding walk (SAW). In this process the random walker has to keep track of the whole history of his path while he moves along, since he is not allowed to visit a site twice. Intuitively, this “long-range repulsive interaction” along the path should make the overall displacement grow stronger with increasing t than in the case of the Bm [79].

Fractional Brownian motion (fBm) is another example. It was introduced by Mandelbrot and van Ness [] to account for processes obeying a scaling law of the functional form $MSD = kt^{2H}$, with $0 < H < 1$, $H \neq \frac{1}{2}$, where $H = \frac{1}{2}$ is the special case of Bm (cfr. Box 11).

It is described by the propagator

$$P(x, t) = \frac{1}{\sqrt{4\pi Dt^{2H}}} \exp \left[-\frac{x^2}{4Dt^{2H}} \right]. \quad (78)$$

fBm has been used as a mathematical reference for random-walk analysis of fixational eye movements (FEMs) and for studying their correlations across time (e.g., [37]). Also, properties of persistence / antipersistence have been exploited, for instance, in analysing optokinetic nystagmus (OKN, [105]).

6.1.1 Case study: random walk analysis of microsaccades

In a number of studies, Engbert and colleagues, e.g., [36, 37, 65] have shown that a typical trajectory generated by the eyes during FEMs exhibits clear features of a random walk.

For instance, on a short time scale (2 to 20 ms), the RW is persistent, whereas on a long time scale (100 to 800 ms) it exhibits anti-persistent behavior. Thus, they observed a time-scale separation with two qualitatively different types of motion. On the short time scale, drift produces persistence and this tendency is increased by the presence of microsaccades. On the long time scale, the anti-persistent behavior is specifically created by microsaccades. Since the persistent behavior on the short time scale helps to prevent perceptual fading and the anti-persistent behavior on the long time scale is error-correcting and prevents loss of fixation, they concluded that microsaccade are optimal motor acts to contribute to visual perception

A more recent model of FEMs has also incorporated self-avoidance as the key mechanism driving drifts observed in fixation tasks [37]. The SAW model encodes history by treating space as a lattice and recording the number of visits to each site: the SAW proceeds by choosing the least-visited neighbor at each step. The model also includes a confining potential to keep the random walk near the origin, which is needed for the long-time subdiffusive nature of fixation tasks, as well as a mechanism for triggering microsaccades when occupying highly-visited sites.

6.1.2 Case study: optokinetic nystagmus

OKN is a reflexive eye movement with target-following slow phases (SP) alternating with oppositely directed fast phases (FP). Trillenber *et al* [105] by measuring FP beginning and ending positions, amplitudes, and intervals and SP amplitudes and velocities, tried to predict future values of each parameter on the basis of past values, using state-space representation of the sequence (time-delay embedding) and local second-order approximation of trajectories. Since predictability is an indication of determinism, this approach allows to investigate the relative contributions of random and deterministic dynamics in OKN. FP beginning and ending positions showed good predictability, but

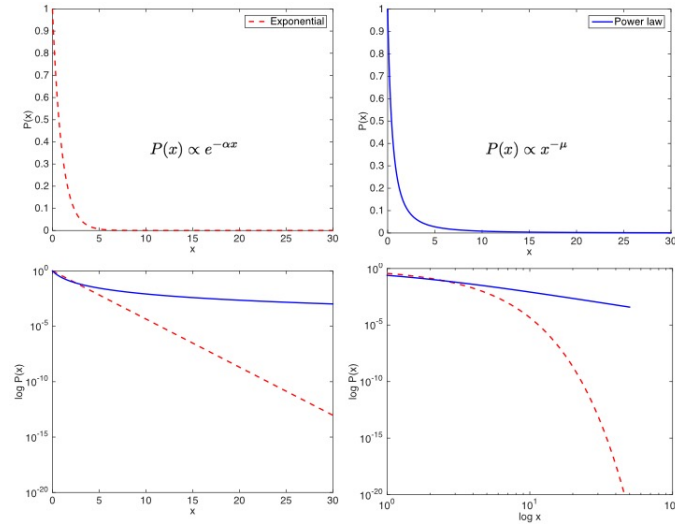


Fig. 23 Exponential distribution $P(x) \propto e^{-\alpha x}$ (top-left) vs. power-law distribution $P(x) \propto x^{-\mu}$ (top-right): pdf shapes look apparently similar. However, the exponential pdf is represented as a straight line on a semilog graph of $\log P(x)$ versus x (bottom-left), whilst the power-law shapes as a straight line on a log-log graph (bottom-right), a signature of the heavy-tail behaviour

SP velocity was less predictable. FP and SP amplitudes and FP intervals had little or no predictability. FP beginnings and endings were as predictable as randomized versions that retain linear auto-correlation; this is typical of random walks. Predictability of FP intervals did not change under random rearrangement, which is characteristic of a random process. They concluded that there is undoubtedly a gross level of deterministic behavior in OKN. Yet within this range, there is apparently significant random behavior, with a small amount of predictability. The random behavior has overlaid on it a form of long-term correlation in the form of anti-persistence. This mixture of dynamics is intriguing and provides a challenge for mathematical modeling efforts, though the physiological meaning of these dynamics is open to conjecture.

6.2 A second violation: losing your moments

Even in the absence of correlations, a mechanism for disrupting convergence to Brownian motion in the long time limit is using power-law tailed distributions in the random walk steps (i.e., power-law distributed noise rather than Wiener or similar noise). **Lévy flights** (LFs) are one such mechanism. LFs

Table 13 Power-law distribution

Many empirical quantities cluster around a typical value: speeds of cars on a highway, the temperature in Freiburg at noon in February, etc. Distributions of these quantities place a negligible amount of probability far from the typical value, making the typical value representative of most observations. In short, the underlying processes that generate these distributions fall into the general class well-described by the CLT.

Not all distributions fit this pattern, however, and in some cases the deviation is not a defect or problem, but rather an indication of interesting underlying complexity in the generating process. Complex social, biological and technological systems give rise to countless example of “non-normal” and **heavy-tailed** distributions. A power-law distribution is one such kind of probability distribution. There are several ways to define them mathematically, one way, for a continuous random variable is the following:

$$P(x) = Cx^{-\mu}, x \geq x_{min}, \quad (79)$$

where $C = (\mu - 1)x_{min}^{\mu-1}$. Note that this expression only makes sense for $\mu > 1$, which is indeed a requirement for a power-law form to normalize.

Power-law distributions have many interesting mathematical properties. Many of these come from the extreme right-skewness of the distributions and the fact that only the first $(\mu - 1)$ moments of a power-law distribution exist; all the rest are infinite. In general, the k th moment is defined as:

$$\begin{aligned} \langle x^k \rangle &= \int_{x_{min}}^{\infty} x^k P(x) dx \\ &= \frac{(\mu - 1)}{x_{min}^{\mu-1}} \int_{x_{min}}^{\infty} x^{-\mu+k} dx = x_{min}^k \left(\frac{\mu - 1}{\mu - 1 - k} \right), \mu > k + 1 \end{aligned} \quad (80)$$

Thus, when $1 < \mu < 2$, the first moment (the mean or average) is infinite, along with all the higher moments. When $2 < \mu < 3$, the first moment is finite, but the second (the variance) and higher moments are infinite! In contrast, all the moments of the vast majority of other pdfs are finite.

Another interesting property of power-law distributions is **scale invariance**. If we compare the densities at $P(x)$ and at some $P(cx)$, where c is some constant, they are always proportional, i.e. $P(cx) \propto P(x)$. This behavior shows that the relative likelihood between small and large events is the same, no matter what choice of “small” we make. That is, the density “scales.”

This behaviour can be seen if we take the logarithm of both sides of Eq. (81)

$$\ln P(x) = \ln C - \mu \ln x \quad (81)$$

That is, rescaling $x \rightarrow cx$ simply shifts the power-law up or down on a logarithmic scale. This shows another of the more well-known properties of a power-law distribution: it appears as a straight line on a log-log plot. This is in contrast to the strongly curved behavior of, say, an exponential distribution (see Fig 23).

The most work has focused on power-law distributions because these have special mathematical properties and can be produced by interesting endogenous processes like feedback loops, self-organization, network effects, etc.

Inspiring analyses of eye movements and visual search in terms of power-law behaviour and power spectra have been conducted by Deborah Aks et al. [1] suggesting that suggest that our oculomotor system may produce a complex and self-organizing search pattern providing maximum coverage with minimal effort.

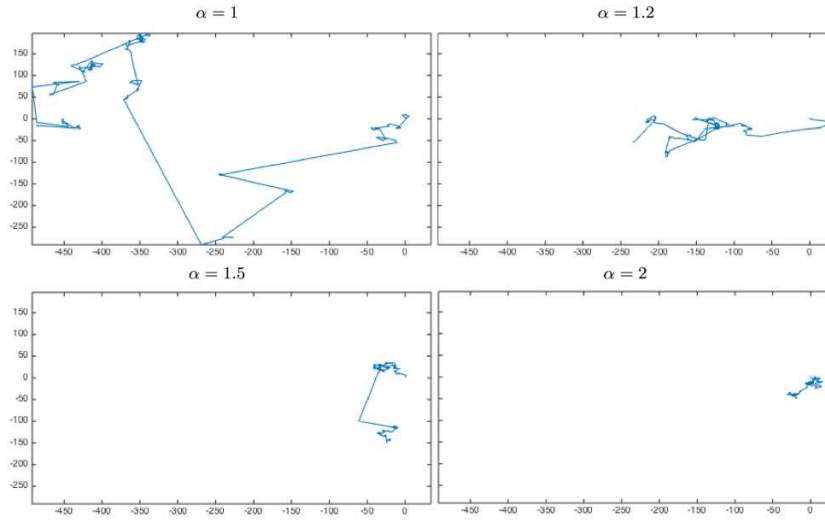


Fig. 24 Different α -stable motions obtained by sampling the “noise” component $\xi \sim f(\xi; \alpha, \beta, \gamma, \delta)$ in Eq. (83) for different values of the characteristic index parameter α . The plots shown in the four panels – left to right, top to bottom –, have been generated via $\alpha = 1, \alpha = 1.2, \alpha = 1.5, \alpha = 2$, respectively. The same number of discrete steps (#500) has been fixed for all the examples, but note how the “scale” of the exploration restricts as $\alpha \rightarrow 2$, eventually reaching the limit case $\alpha = 2$ where classic Bm is generated (bottom right panel).

are stochastic processes characterized by the occurrence of extremely long jumps, so that their trajectories are not continuous anymore. The length of these jumps is distributed according to a Lévy stable statistics with a power-law tail and divergence of the second moment. This peculiar property strongly contradicts the ordinary Brownian motion, for which all the moments of the particle coordinate are finite.

For a random walker who takes steps of size l according to a probability density function

$$P(l) \approx l^{-\mu} \quad (82)$$

the resulting type of diffusion depends on the value of μ . In particular:

- a) $\mu > 3$: the CLT guarantees convergence to normal diffusion and Brownian regime holds;
- b) $\mu \rightarrow 1$: the ballistic motion limit is reached;
- c) $1 < \mu < 3$: superdiffusive behaviour occurs.

LFs arise in the super diffusive regime, when the jump size distribution has a power-law tail with $\mu < 3$. As discussed in Box 13, for such values of the power-law exponent, the RVs can have diverging variance. The necessary and sufficient conditions of the CLT do not hold in this case. Lévy flight patterns comprise sequences of randomly orientated straight-line movements.

Frequently occurring but relatively short straight-line movement randomly alternate with more occasionally occurring longer movements, which in turn are punctuated by even rarer, even longer movements, and so on with this pattern repeated at all scales. Some examples of LF patterns are provided in Figure 24. As a consequence, the straight-line movements have no characteristic scale, and LFs are said to be **scale-free**.

At the microscopic level, the simulation of individual LF trajectories do not require complex calculations to execute. They are a Markovian process and can be easily obtained from Eq. 48, by setting $\mathbf{A} = 0$

$$d\mathbf{x}(t) = \mathbf{B}(\mathbf{x}, t)\boldsymbol{\xi}(t)dt = \mathbf{B}(\mathbf{x}, t)d\mathbf{L}_\alpha(t) \quad (83)$$

This is formally equivalent to the Wiener process, however in this case the stochastic increment $d\mathbf{L}_\alpha(t) = \boldsymbol{\xi}(t)dt$ is sampled from an α -**stable distribution** $f(\boldsymbol{\xi}; \alpha, \beta, \gamma, \delta)$ (cfr. Table 14):

$$\boldsymbol{\xi}(t) \sim f(\boldsymbol{\xi}; \alpha, \beta, \gamma, \delta). \quad (84)$$

In other terms, $d\mathbf{L}_\alpha(t)$ in the context of Eq. 83 represents an infinitesimal Lévy motion.

The macroscopic description of the pdfs for particles undergoing a Lévy flight can be modeled using a generalized version of the Fokker-Planck equation. The equation requires the use of fractional derivatives and we will not discuss it here since really beyond the scope of an introductory chapter.

By discretising and iterating Eq. 83, over a large number of trials a Lévy flight will be distributed much farther from its starting position than a Brownian random walk of the same length (see again Figure 24). Indeed, the *MSD* of a Brownian walker has a linear dependence on time whereas that of a Lévy flier grows faster and depends on time raised to some power > 1 . This result gives a precise meaning to their characterisation as “super-diffusive.” The probability density function for the position of the walker converges to a Lévy α -stable distribution with Lévy index $\alpha = \mu - 1$, with $0 < \alpha \leq 2$ (with the special case $\alpha = 2$ corresponding to normal diffusion).

The Hurst exponent H , the characteristic index α , and the power-law exponent μ are related as follows:

$$H = \frac{1}{\alpha} = \frac{1}{\mu - 1} \quad (85)$$

characterizes the behavior.

Thus, rephrasing the conditions that have been discussed for the μ exponent, for $\alpha < 2$ one cannot define the MSD because it diverges. Instead, one can study moments of order lower than α because they do not diverge. Nevertheless, one can define some “empirical” width, such as half widths at half maximum, and show that a *pseudo*-MSD grows as $\approx t^{\frac{1}{\alpha}}$ for Lévy flights.

Table 14 Stable distributions

The family of α -stable distributions [43] form a four-parameter family of continuous probability densities, say $f(\xi; \alpha, \beta, \gamma, \delta)$. The parameters are the skewness β (measure of asymmetry), the scale γ (width of the distribution) and the location δ and, most important, the **characteristic exponent** α , or index of the distribution that specifies the asymptotic behavior of the distribution. The relevance of α derives from the fact that the pdf of jump lengths scales, asymptotically, as $l^{-1-\alpha}$. Thus, relatively long jumps are more likely when α is small. By sampling $\mathbf{x} \sim f(x; \alpha, \beta, \gamma, \delta)$, for $\alpha \geq 2$ the usual Bm occurs; if $\alpha < 2$, the distribution of lengths is “broad” and the so called Lévy flights take place.

One example of α -stable motions generated for varying the α index is illustrated in Figure 24.

A random variable X is said to have a stable distribution if the parameters of its probability density function (pdf) $f(x; \alpha, \beta, \gamma, \delta)$ are in the following ranges $\alpha \in (0; 2]$, $\beta \in [-1; 1]$, $\gamma > 0$, $\delta \in \mathbb{R}$ and if its characteristic function $E[\exp(itx)] = \int_{\mathbb{R}} \exp(itx) dF(x)$, F being the cumulative distribution function (CDF), can be written as

$$E[\exp(itx)] = \begin{cases} \exp(-|\gamma t|^\alpha) (1 - i\beta \frac{t}{|t|} \tan(\frac{\pi\alpha}{2}) + i\delta t) \\ \exp(-|\gamma t| (1 + i\beta \frac{2}{\pi} \frac{t}{|t|} \ln|t|) + i\delta t) \end{cases}$$

the first expression holding if $\alpha \neq 1$, the second if $\alpha = 1$.

Special cases of stable distributions whose pdf can be written analytically, are given for $\alpha = 2$, the **Normal distribution** with

$$f(x; 2, 0, \frac{\sigma}{\sqrt{2}}, \mu) = \mathcal{N}(x; \mu, \sigma^2), \quad (86)$$

for $\alpha = 1$, the **Cauchy or Lorentz distribution**

$$f(x; 1, 0, \gamma, \delta) = \frac{1}{\pi\gamma} \left[\frac{\gamma^2}{(x - \delta)^2 + \gamma^2} \right], \quad (87)$$

and for $\alpha = 0.5$, the **Lévy distribution**

$$f(x; 0.5, 1, \gamma, \delta) = \sqrt{\frac{\gamma}{2\pi}} \frac{\exp(-\frac{\gamma}{2(x-\delta)})}{(x-\delta)^{3/2}}. \quad (88)$$

For all other cases, only the characteristic function is available in closed form, and numerical approximation techniques must be adopted for both sampling and parameter estimation [21, 75, 61]. A very nice and simple to use Matlab package for parameter inference and computation of α -stable distributions is freely downloadable at Mark Veillette’s homepage <http://math.bu.edu/people/mveillet/html/alphastablepub.html>.

Some examples of α -stable pdfs and related **complementary cumulative distribution function** (CCDF) are given in Fig.25. The use of the CCDF, or upper tail, of jump lengths is the standard convention in the literature, for the sake of a more precise description of the tail behaviour, i.e. the laws governing the probability of large shifts. This can be defined as $\overline{F}(x) = P(X > x) = 1 - F(x)$, where F is the CDF.

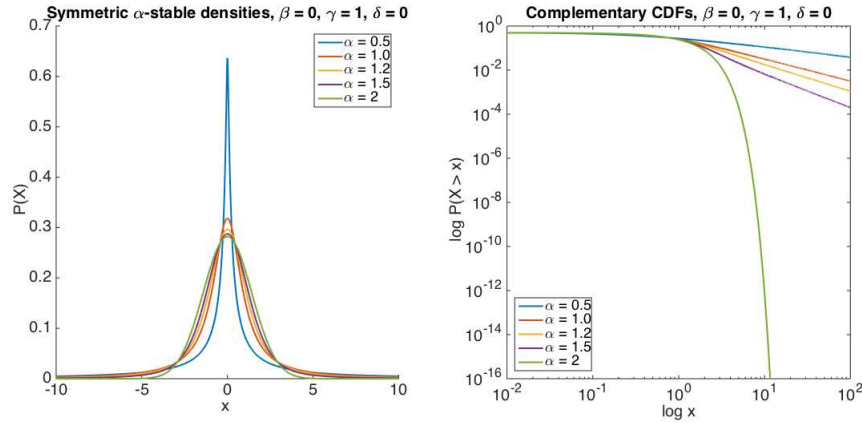


Fig. 25 Plots of symmetric α -stable distributions (left) and their complementary CDF (CCDF) on log – log axes (right) for different values of the characteristic index parameter $\alpha = 0.5, 1, 1.2, 1.5, 2$. The CCDF shows the rapid fall-off of the tail of the Gaussian case ($\alpha = 2$) as opposed to the power-law tail behaviour of actual Lévy flights $\alpha < 2$

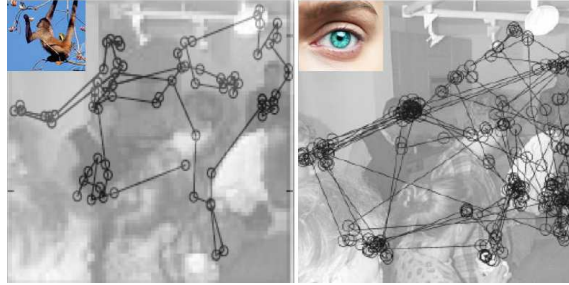
6.2.1 Case study: the Lévy flight of saccades

Brockmann and Geisel [14] have assumed a power-law dependence in the tail of the saccade amplitude distribution, for which they found empirical support in free viewing of natural scenes. Minimization of the time needed to scan the entire visual space then led them to predict that eye movement trajectories behave as Lévy flights, as opposed to more common diffusive random walks, which would result from a Gaussian amplitude distribution. But in order to obtain simulated eye trajectories that look like their observed scanpaths, an empirical determination of a salience field for the correspondingly viewed scene is still needed. Brockmann and Geisel derived that salience field from the spatial distribution of fixations made by observers throughout the scene (a picture of a party). As to the amplitude distribution they considered the Cauchy distribution (Eq. 87)

The stochastic assumptions of saccade generation made by Brockmann and Geisel [14] involve a Markovian process, consistent with an interpretation of visual search originally proposed by Horowitz and Wolfe [52]. However, the predictions and results of the Brockmann and Geisel model do not change substantially if those assumptions are relaxed so as to allow a sufficiently rapidly decaying correlation in the saccade sequences.

Further evidence and characterization of Lvy-like diffusion in eye movements associated with spoken-language comprehension have recently been provided by Stephen, Mirman, Magnuson, and Dixon [95].

Fig. 26 Monkey or human: can you tell the difference? The left image has been obtained by superimposing a typical trajectory of spider monkeys foraging in the forest of the Mexican Yucatan, as derived from [84], on the “party picture” used in [14]. The right image is an actual human scan path (modified after [14])



6.2.2 Case study: the microsaccade conundrum

Martinez-Conde and colleagues [69, 76] have put forward the proposal that microsaccades and saccades are the same type of eye movement (the “continuum hypothesis”) The microsaccade–saccade continuum is sustained by evidence that saccades of all sizes share a common generator

In this respect, a straightforward hypothesis on the function microsaccades is that they help to scan fine details of an object during fixation. This hypothesis would imply that fixational eye movements represent a search process. According to this analogy, the statistics of microsaccades can be compared to other types of random searches, namely inspection saccades during free picture viewing [14].

Given these assumptions, Engbert et al. checked whether the amplitude distribution of microsaccades and saccades follows a similar law.

To investigate the distribution of microsaccade amplitude in a data set of 20.000 microsaccades, they analyzed the tail of the distribution on a double logarithmic scale. They obtained a power-law decay of the tail with exponent $\mu = 4.41$, which would reject the hypothesis of a Levy flight for microsaccades (requiring $\mu < 3$), if compared with numerical results obtained by Brockmann and Geisel [14]. In turn, this apparently would also lead to reject the “continuum hypothesis”. However there are many subtleties that should be taken into account in order to fairly compare two such different analyses (e.g., sampling rate and discretisation of the eye tracking raw data) before reaching a conclusion. But at least this nice piece of work is useful to show how advanced statistical methods for eye movement analysis can address big questions in the field.

6.3 The foraging perspective

Consider Figure 26: *prima facie*, it seems to illustrate a bizarre jest. However, from eye-movements studies [17, 98, 100, 101, 31, 77, 99], there is evidence that eye movement trajectories and their statistics are strikingly similar, with respect to the resulting movement patterns and their statistics to those exhibited by foraging animals, [108, 25, 81, 89]. In other terms, eye movements and animal foraging address in some way a similar problem [14]. Under the foraging metaphor, the eye (and the brain modules controlling the eye behavior) is the forager, the input visual representation \mathcal{D} is the foraging landscape, points attracting fixations are foraging sites or moving preys; gaze shifts occur due to local exploration moves, prey pursuit and long relocation from one site to another.

An intriguing issue is whether the foraging theory underpinning the proposed analyses just provides a useful computational theory metaphor, or a constitutes a more substantial ground. Interestingly enough, Hills [50] has argued that what was once foraging in a physical space for tangible resources became, over evolutionary time, foraging in cognitive space for information related to those resources. Adaptations that were selected for during ancestral times are, still adaptive now for foraging on the internet or in a supermarket, or for goal-directed deployment of visual attention [113]. In these terms, the foraging approach may set a broader perspective for discussing fundamental themes in eye movement behavior, e.g., the “continuum hypothesis” of Martinez-Conde and colleagues [69, 76].

Building on this rationale, gaze shift models have been proposed coping with different levels of visual representation complexity [4, 6, 7, 8, 24, 74] and eye movement data analyses have been performed in terms of foraging efficiency [113, 16].

Rewrite the Langevin equation (48), interpreting the deterministic component $\mathbf{A}(\mathbf{x}, t)$ as an external force field due to a potential $V(\mathbf{x}, t)$ [4] (see Fig. 27), that is $\mathbf{A}(\mathbf{x}, t) = -\nabla V(\mathbf{x}, t)$, where the “del” (or “nabla”) symbol ∇ denotes the gradient operator⁵.

Then,

$$d\mathbf{x}(t) = -\nabla V(\mathbf{x}, t)dt + \mathbf{B}(\mathbf{x}, t)d\mathbf{L}_\alpha(t). \quad (89)$$

Equation 89 now provides a microscopic description (trajectory) of a RW biased by an external force field.

We can thus generalise to $2 - D$ the discretisation method used to obtain the $1 - D$ Eq 53 so to gain an operative definition of the SDE (89)

⁵ A salience map, and thus the potential field V derived from salience, varies in space (as shown in Fig. 27). The map of such variation, namely the rate of change of V in any spatial direction, is captured by the vector field ∇V . To keep things simple, think of ∇ as a “vector” of components $(\frac{\partial}{\partial x}, \frac{\partial}{\partial y})$. When ∇ is applied to the field V , i.e. $\nabla V = (\frac{\partial V}{\partial x}, \frac{\partial V}{\partial y})$, the gradient of V is obtained

$$\underbrace{\mathbf{x}_{i+1}}_{\text{new gaze location}} = \underbrace{\mathbf{x}_i}_{\text{current gaze location}} - \underbrace{\nabla V(\mathbf{x}_i, t_i) \Delta t_i}_{\text{external force}} + \underbrace{\mathbf{B}(\mathbf{x}_i, t_i) (\Delta t_i)^{\frac{1}{\alpha}} \boldsymbol{\xi}_i}_{\text{Lévy motion}} \quad (90)$$

which makes clear that next gaze position is obtained by shifting from current gaze position following a Lévy displacement that is constrained by the external potential field. The external potential summarizes the informative properties of the “visual landscape” of the forager.

For instance in [4] Eq. (90) was used as a *generative model* of eye movements. In that case, the external potential was taken as a function of the salience field and $\boldsymbol{\xi}_i$ was sampled from a Cauchy distribution. One example is provided in Figure 27 (Matlab software for the simulation is freely downloadable at <http://www.mathworks.com/matlabcentral/fileexchange/38512>).

It is worth noting, as to parameters of Eq. (90) that are available established numerical techniques for fitting such parameters from real data (see, e.g. [94])

As previously discussed, the heavy-tailed distributions of gaze shift amplitudes are close to those characterizing the foraging behavior of many animal species. Lévy flights have been used to model optimal searches of foraging animals, namely their moment-to-moment relocations/flights used to sample the perceived habitat [108]. However, the general applicability of Lévy flights in ecology and biological sciences is still open to debate. In complex environments, optimal searches are likely to result from a *composite strategy*, in which Brownian and Lévy motions can be adopted depending on the structure of the landscape in which the organism moves [81]. Lévy flights are best suited for the location of randomly, sparsely distributed patches and Brownian motion gives the best results for the location of densely but random distributed within-patch resources [88].

Also it is possible to compose the strategy as a hybrid strategy in which Brownian-like motion is adopted for local exploration (e.g., FEMs and small saccades) and Lévy displacements are exploited for long relocations (medium / long saccades) A preliminary attempt towards such a composite strategy for modelling gaze shift mechanisms has been presented in [5]. However, that approach only conjectured a simple binary switch between a Gaussian and a Cauchy-like walk. In [8] the approach was generalised to handle observers watching videos and thus accounting for multiple kinds of shifts: FEMs, saccade and smooth pursuit (cfr. Figure 28). To this end, Eq. (90) is reformulated as a two-dimensional dynamical system in which the stochastic part is driven by one-of- K possible types of α -stable motion $\boldsymbol{\xi}_i^k$.

In the Ecological Sampling model [8] the switch from one motion type to the other was bottom-up determined as a multinomial choice biased by the complexity of the sampled visual landscape. More recently this idea was extended to a top-down and task-dependent probabilistic choice in the framework of Bayesian Decision theory [24].

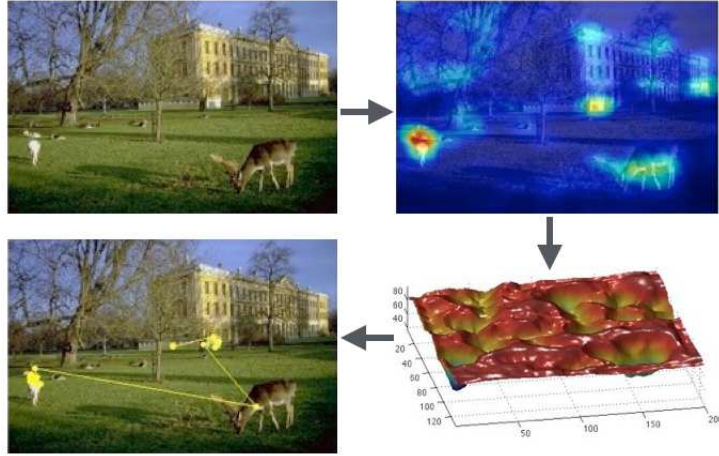
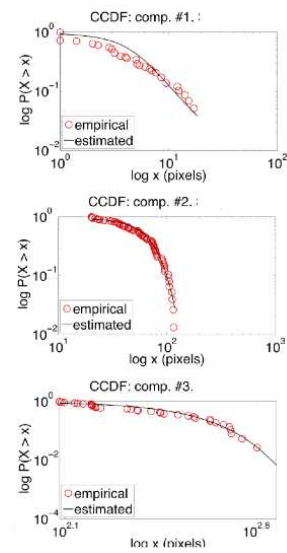


Fig. 27 The Lévy model used as a generative model. Top left: the original image. Top right: the saliency map. Bottom right: the potential $V(\mathbf{x}_i, t_i)$ computed from saliency: *potential wells* represent informative regions that can attract gaze. Bottom, left: the final scan path superimposed on the original image.

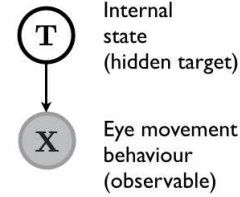
Fig. 28 Analysis of gaze shift dynamics from a video. The different components were automatically separated by using a clustering procedure based on the Variational Expectation-Maximization algorithm (see [8] for details). Then, each component was fitted by an α -stable distribution. Fitting results for one eye-tracked subject are shown in terms of double log plot of the CCDF. From top to bottom: first component accounting for smooth-pursuit and FEMs motions; the medium saccade component; the long saccade component



7 From patterns of movement to patterns of the mind: unveiling observer's hidden states

The last point we are addressing in this Chapter is: can we infer target hidden states of observer's mind by analyzing his eye movement trajectories?

Fig. 29 The PGM specifying the generative process $\mathbf{T} \rightarrow \mathbf{X}$ through the joint pdf factorization: $P(\mathbf{T}, \mathbf{X}) = P(\mathbf{X} | \mathbf{T})P(\mathbf{T})$. The shaded node denotes that RV \mathbf{X} is observable



Or, in foraging terms, can we say something on forager’s internal state by observing his foraging patterns? Generally speaking, the hidden states that we may target could be, for example, the task the observer is accomplishing, his expertise, his emotional state (but, also, a certain pathology affecting a group of patients as opposed to a control group).

More formally, if \mathbf{T} denotes the target internal state (or a set of states) and \mathbf{X} the visible eye movement behavior, e.g., $\mathbf{X} = \{\mathbf{x}_F(1), \mathbf{x}_F(2), \dots\}$, (or, alternatively, the sequence of gaze, amplitudes, directions and durations), one can assume a generative process $\mathbf{T} \rightarrow \mathbf{X}$, where the observer’s hidden state shapes the kind of eye trajectories.

In probabilistic terms the generative process can be captured by the simple PGM sketched in Figure 29, which factorizes the joint pdf $P(\mathbf{T}, \mathbf{X})$ as $P(\mathbf{T}, \mathbf{X}) = P(\mathbf{X} | \mathbf{T})P(\mathbf{T})$ (product rule).

This way, anything we can infer on the hidden state given the observable behavior is obtained by “inverting the arrow”, i.e., by applying Bayes’rule:

$$P(\mathbf{T} | \mathbf{X}) = \frac{P(\mathbf{X} | \mathbf{T})P(\mathbf{T})}{P(\mathbf{X})}. \quad (91)$$

Once the posterior has been computed, then we use decision theory to determine output $\mathbf{T} = t$ for each new input $\mathbf{X} = \mathbf{x}$

Note that this is a very general formulation of the problem, which actually may entail a large number of solutions, and the PGM shown in Figure 29 could be further specified/specialized in number of ways. Also, to keep the description simple, we have omitted the set of parameters involved by the actual specification of the pdfs in Eq. 91. Clearly, before Eq. 91 can be put into work, such parameters are to be specified and fitted, or, adopting a more modern term, learned. To this end, a huge amount of Machine Learning (ML) techniques are today available (see Table 15, for ML basic terminology in a nutshell, and [3, 72] for an in-depth presentation)

However, keeping to such general level, from a methodological standpoint there are at least three distinct approaches to cope with the inverse inference problem posed by Eq. 91. These are given, in decreasing order of complexity, by:

1. First solve the inference problem of determining the likelihood function $P(\mathbf{X} | \mathbf{T})$ and the prior probabilities $P(\mathbf{X})$. Then use Bayes’ theorem in the form given in Eq. 91. Equivalently, we can model the joint distribution

$P(\mathbf{T}, \mathbf{X})$ directly and then normalize to obtain the posterior probabilities. Approaches that explicitly or implicitly model the distribution of inputs as well as outputs are known as *generative models*, because by sampling from them it is possible to generate synthetic data points in the input space. The popular Naive Bayes and Linear Discriminant Analysis methods are very simple instances (though effective in many practical cases) of a generative approach; Hidden Markov Models (HMM) [3, 72] for modeling time series provide an appealing example of a generative approach that has been often exploited for eye movement analysis.

2. Solve straightforwardly the inference problem of determining the posterior probabilities, and then subsequently use decision theory to assign each new $\mathbf{X} = \mathbf{x}$ to an output target. Approaches that model the posterior probabilities directly are called *discriminative models*. Logistic regression is one notable and classic example, Conditional Random Fields (CRFs) for modeling time series are more sophisticated one [3, 72].
3. Find a function $f : \mathbf{X} \rightarrow \mathbf{T}$, called a *discriminant function*, which maps each input $\mathbf{X} = \mathbf{x}$ directly onto a class label. For instance, in the case of two-class problems, e.g., distinguishing experts from naive observers, \mathbf{T} might be binary valued and such that $f = 0$ represents class $\mathbf{T} = t_1$ and $f = 1$ represents class $\mathbf{T} = t_2$. In this case, probabilities play no role. Many popular artificial neural nets or modern methods such as the Support Vector Machine (SVM) for regression and classification (a baseline technique in ML) implement this approach [3, 72].

Note that, since many applications require a posterior class probability, methods based on discriminant functions can be “transformed” into discriminative ones in order to gain an output in probabilistic form. For instance, the output $f(\cdot)$ of binary SVM classifier can be fed into a sigmoid function, to approximate the posterior (e.g., $P(\mathbf{t} | \mathbf{X}) \approx \frac{1}{1 + \exp(Af + B)}$, where A, B are parameters that can be determined via regularized maximum likelihood).

Clearly, the generative approach is in principle the most appealing one. However it should be recalled that apart from simple cases such as Naïve Bayes (see Table 16), the normalization of the joint pdf can be a hard task. Referring again to Eq. 91, calculating the normalization factor $P(\mathbf{X})$ requires the marginalization $P(\mathbf{X}) = \sum_{\mathbf{T}} P(\mathbf{T}, \mathbf{X})$ ($P(\mathbf{X}) = \int P(\mathbf{T}, \mathbf{X}) d\mathbf{T}$ when RVs are continuous), which, in real cases, is hardly computable. Thus, complex approximation techniques such as Monte Carlo or Variational Bayes are to be taken into account [3, 72].

7.1 Inverting Yarbus to infer the task

When \mathbf{T} represents a given task, Eq. 91 formalizes the inference of the on-going task by observing the eye movements of the viewer. After the seminal

Table 15 Machine Learning in a nutshell

In the inferential process defined by Eq. 91, \mathbf{T} represents the output of the process and \mathbf{X} the given input. In statistical Machine Learning (ML) terminology \mathbf{X} is usually shaped as a random vector of features (or attributes, or covariates), $\mathbf{X} = \{\mathbf{X}_i\}_{i=1}^N$, where i is a suitable index. For example when i is a time index, then $\{\mathbf{x}_1, \mathbf{x}_2\}$ is the realization of a a stochastic process. ML does not relate to a specific problem thus \mathbf{X}_i could be a complex structured object, such as an image, a sentence, an email message, a graph, etc.

The form of the output or response variable \mathbf{T} can be either discrete (categorical, nominal) or continuous (real-valued). One example of the first type, is when \mathbf{T} can take the label of one of two tasks given to the observer, e.g., $\mathbf{T} = t_k$ where $t_1 = \text{“look for people”}$ and $t_2 = \text{“look for cars”}$. Another example, is \mathbf{T} taking values over the discrete set of basic emotion (“fear”, “disgust”, “joy”, etc.). As opposed to this latter example, we could try instead, to infer from eye movements a continuous affect state, so that \mathbf{T} is taking values t_i in the real valued space of arousal.

From a practical standpoint, when using a ML approach to analyze our eye tracking data we can be in one of these two conditions:

1. **supervised learning**: we know where input \mathbf{x}_i comes from (e.g., \mathbf{x}_i was measured while the observer was scanning a happy face); more formally \mathbf{x}_i is paired with target value or label t_i , thus we have a training set $\mathcal{D} = \{(\mathbf{x}_i, t_i)\}_{i=1}^N$;
2. **unsupervised learning**: we have no labels, and our dataset is represented by the bare input data $\mathcal{D} = \{\mathbf{x}_i\}_{i=1}^N$

Thus, in the supervised setting the goal is to learn a mapping from input \mathbf{X} to output \mathbf{T} , given a labeled set of input-output pairs. When \mathbf{T} is discrete the problem is known as **classification** or pattern recognition; when \mathbf{T} is real-valued, we are performing **regression**.

In the unsupervised setting, we have no labels available, thus the goal is to find “interesting patterns” in the data. This is sometimes named knowledge discovery or data mining. It is a much less well-defined problem, since we are not told what kinds of patterns to look for, and there is no obvious error metric to use (unlike supervised learning, where we can compare our prediction for a given \mathbf{x} to the observed value). When \mathbf{T} is discrete, the problem is known as **clustering**. When \mathbf{T} is real-valued we are typically in the case of **dimensionality reduction**. The latter is used when dealing with high dimensional data: it is often useful to reduce the dimensionality by projecting the data to a lower dimensional subspace which captures the “essence” of the data. Indeed, although the input data may appear high dimensional, there may only be a small number of degrees of variability, corresponding to **latent factors** (Principal Component Analysis or Factor Analysis being well known examples).

Statistical Machine Learning is nowadays a broad and mathematically sophisticated field. Two excellent and up-to-date textbooks are those by Bishop [3] and Murphy [72].

		Supervised (with labels)	Unsupervised (no labels)
T	Discrete (categorical)	classification or categorization (pattern recognition)	clustering (knowledge discovery)
	Continuous (real valued)	regression	dimensionality reduction (latent factors discovery)

Fig. 30 The main problems Machine Learning is addressing

experiment by Yarbus [114] - who studied the effect of visual task on trajectories of eye movements, which in Eq. 91 is formally captured by the likelihood function $P(\mathbf{X} | \mathbf{T})$ capturing the forward mapping $\mathbf{T} \rightarrow \mathbf{X}$ -, inferring the inverse mapping $\mathbf{X} \rightarrow \mathbf{T}$, i.e. computing the posterior $P(\mathbf{T} | \mathbf{X})$ has been named “inverse Yarbus” process [45].

Clearly, as previously mentioned, there are several ways of inverting Yarbus.

7.1.1 Case study: Inverting Yarbus via Naïve Bayes

In a recent study [49], Henderson *et al.* considered four tasks: scene search, scene memorization, reading, and pseudo-reading. Task inference was achieved by classifying the observers’ task by implementing Eq. 91 as the baseline Naïve Bayes’ (NB) classifier. Namely they addressed two problems: (i) whether the task associated with a trial could be identified using training from other trials within the same experimental session (within-session classification); (ii) whether the task performed in one session could be identified based on training from a session conducted on a different day (cross-session classification). Twelve members of the University of South Carolina community participated in the experiment. A dedicated classifier was trained for each observer, thus the baseline NB has proved to be sufficient. NB classifiers were trained on a feature vector \mathbf{X} of dimension 8, i.e., eight eye movement features capturing eye movement patterns for each trial: the mean and standard deviation of fixation duration, the mean and standard deviation of saccade amplitude, the number of fixations per trial, and the three parameters μ , σ , and τ quantifying the shape of the fixation duration distribution with an ex-Gaussian distribution, which is known to change for different eye-movement tasks (cfr., [49] for details).

Table 16 Naïve Bayes

The Naïve Bayes algorithm is a classification algorithm based on Bayes rule, that assumes the attributes $\mathbf{X} = \{\mathbf{X}_1, \mathbf{X}_2, \dots\}$ are all conditionally independent of one another given \mathbf{T} . Consider, for example, the two feature case, where $\mathbf{X} = \{\mathbf{X}_1, \mathbf{X}_2\}$, then

$$P(\mathbf{X} | \mathbf{T}) = P(\mathbf{X}_1, \mathbf{X}_2 | \mathbf{T}) = P(\mathbf{X}_1 | \mathbf{X}_2, \mathbf{T})P(\mathbf{X}_2 | \mathbf{T}) = P(\mathbf{X}_1 | \mathbf{T})P(\mathbf{X}_2 | \mathbf{T}) \quad (92)$$

Thus, if \mathbf{X} contains n attributes: $P(\mathbf{X} | \mathbf{T}) = \prod_{i=1}^n P(\mathbf{X}_i | \mathbf{T})$. This way Eq. 91 can be written as

$$P(\mathbf{T} = t_k | \mathbf{X}) = \frac{P(\mathbf{T} = t_k) \prod_{i=1}^n P(\mathbf{X}_i | \mathbf{T} = t_k)}{\sum_j P(\mathbf{T} = t_j) \prod_{i=1}^n P(\mathbf{X}_i | \mathbf{T} = t_j)}. \quad (93)$$

If we are interested only in the most probable value of \mathbf{T} , then we have the Naïve Bayes classification/decision rule: $\mathbf{T} \leftarrow \arg \max_{t_k} P(\mathbf{T} = t_k | \mathbf{X})$, which simplifies Eq. 93 to the following (because the denominator does not depend on t_k):

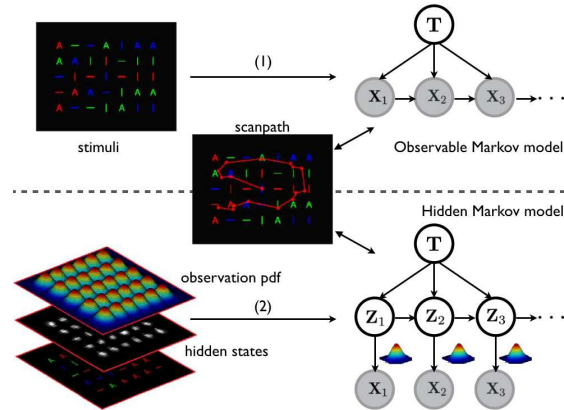
$$\mathbf{T} \leftarrow \arg \max_{t_k} P(\mathbf{T} = t_k) \prod_{i=1}^n P(\mathbf{X}_i | \mathbf{T} = t_k) \quad (94)$$

7.1.2 Case study: Inverting Yarbus via HMM

In [45] Haji-Abolhassani and Clark present a study in which Eq. 91 is shaped to explicitly account for the gaze shift sequence as a stochastic process. They present different experiments and models, but here, for clarity sake, we will consider a basic condition and a baseline model so to capture the rationale behind their approach and, also, to compare with the Ellis and Stark model presented in Section 5.2.1. Recall that in that case the transition matrix A_{kj} was directly estimated by “counting” the percentage of transitions from one point of interest to another (more formally, via Maximum Likelihood estimation). Thus, the model was an observable Markov model. In the inverse Yarbus setting, it can be represented as the Markov chain conditioned on task \mathbf{T} that is depicted in Figure 31 (top panel, solution 1). Different tasks are likely to give rise to different transition matrices. In [45] visual tasks considered in the simplest experiment were: counting red bars, green bars, blue bars, horizontal bars, vertical bars, or characters.

Even if we leave apart subtle issues such as the dissociation between the center of gaze and the covert focus of attention [45], it is very unlikely for a saccade to land exactly on the chosen point of interest (objects or salient locations). The fixation locations may undershoot or overshoot the targets due to oculomotor properties of human eyes or the noisiness of the eye tracker. To account for this problem, in terms of an observable Markov model, a

Fig. 31 Two solutions for the inverse Yarbus given a time series of observations: (1) the task-conditioned observable Markov model [44, 35] (top panel) and the task-conditioned hidden Markov model [45] (bottom panel)



“practical” viable solution is to relax the point of interest condition to a more flexible Region of interest (ROI) centered on the exact point.

As a more principled alternative, one can assume that the true points of interest correspond to “hidden” targets or states: when one such target is chosen at time t , say \mathbf{z}_t , the corresponding actual fixation \mathbf{x}_t will be generated by adding some noise ϵ (e.g., distributed according to a zero mean Gaussian pdf), i.e. $\mathbf{x}_t = \mathbf{z}_t + \epsilon$. In other terms, we are assuming that $P(\mathbf{x}_t | \mathbf{z}_t) = \mathcal{N}(\mathbf{x}_t; \mathbf{z}_t, \Sigma)$. That is, when \mathbf{z}_t is chosen, the actual observation is obtained by sampling from a Gaussian distribution $\mathcal{N}(\mathbf{x}_t; \mathbf{z}_t, \Sigma)$ centered on the true target \mathbf{z}_t , where the inverse of the covariance matrix Σ will define the precision of target shooting.

The corresponding PGM is the Dynamic Bayesian Network depicted in Figure 31 (bottom panel, solution 2), which represents a hidden Markov model conditioned on task \mathbf{T} . The problem of learning such DBN can be further simplified by learning a separate HMM for a given task $\mathbf{T} = t_k$. This way each task will be implicitly defined through the set of parameters defining the corresponding HMM, $\mathbf{T} = t_k \iff \Theta = \Theta_k$ (cfr, Figure 32

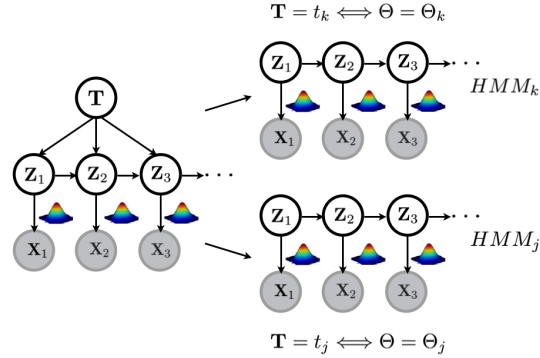
Eventually, task inference is performed by choosing the HMM providing the higher likelihood for the input observation \mathbf{x}_{new} .

A more complex example of how to exploit DBNs for coupling eye movements and hand actions in drawing is provided in Coen-Cagli *et al.* [27, 26].

7.2 Assessing cognitive impairments and expertise

Eq. 91, can be used beyond the important issue of task classification. More generally, the value of \mathbf{T} can represent a label ℓ to identify groups of observers that exhibit different eye movement behaviour with respect to a given task. In these circumstances, Eq. 91 formalizes the probability that one observer

Fig. 32 For K tasks, the problem of learning the parameters for the DBN on the left is simplified to learning K simple HMM parameters. In the learning stage, for each task $\mathbf{T} = t_k$ a specific set of parameter Θ_k is from observations, obtaining the k -th HMM. Task inference is performed by choosing the HMM providing the higher likelihood for the input observation \mathbf{x}_{new}



belongs to one group. The posterior can then be used for classification (e.g., via the arg max decision rule).

7.2.1 Case study: Assessing cognitive impairments

On the rationale that patients with mild cognitive impairment (MCI) often progress to Alzheimer’s disease (AD), Lagun *et al.* [62] applied ML methods to analyze and exploit the information contained in the characteristics of eye movement exhibited by healthy and impaired subjects during the viewing of stimuli in the Visual Paired Comparison (VPC) task for the detection of memory impairment associated with MCI. The VPC assessment proceeds in two steps. During the familiarization phase, subjects are presented with two identical visual stimuli, side by side, on a computer screen. Eye tracked subjects are allowed to look at the pictures for a specified amount of time. During the test phase, subjects are presented with pictures of the old stimulus and a novel stimulus, side by side. Control subjects typically spend 70% of the time during the test phase looking at the novel stimulus, which indicates that they have a memory for the repeated, and now less interesting, stimulus. In contrast, age-matched MCI patients did not spend more time looking at the novel stimulus than the repeated stimulus.

Data analysis was conducted via supervised classification (two class/label problem, \mathbf{T} taking values in $\ell = \{“impaired”, “control”\}$), by exploiting standard techniques, namely Naïve Bayes, Logistic Regression, and the Support Vector Machine. They first trained the classification models on the multidimensional representation \mathbf{X} of eye movements from a sample of the impaired and control subjects, $\mathcal{D} = \{\mathbf{x}_{train}, \ell\}$ and then used the model to predict the status of new subjects based on their eye movement characteristics, i.e., $P(\mathbf{T} | \mathbf{X} = \mathbf{x}_{new})$. The results showed that eye movement characteristics including fixation duration, saccade length and direction, and re-fixation patterns (gaze position re-visits on previously seen parts of the stimuli) can be

used to automatically distinguish impaired and normal subjects. In this study the SVM classifier outperformed the other techniques.

Beyond the specific issue addressed by Lagun *et al.*, it is worth looking at their paper [62] because it provides a gentle introduction to the Naïve Bayes, Logistic Regression, and SVM algorithms.

7.2.2 Case study: Classifying billiard player expertise

The study presented in [10] analyzed the oculomotor behavior of individual observers engaged in a visual task, with the aim of classifying them as experts or novices (two class/label problem, \mathbf{T} taking values in $\ell = \{\text{“expert”}, \text{“naïve”}\}$). To this end, various visual stimuli and tasks were administered to 42 subjects, half novices and half expert billiard players. Stimuli were a portion of a real match, videorecorded from the top, containing several shots of variable length and complexity, as well as a number of ad-hoc individual shots, also videorecorded from the top in a real setting. The match stimulus was associated to a free-viewing observation condition, while for the individual shots, which were occluded in the final part of the trajectory, observers were asked to predict the outcome of the shot, which placed implicitly a significant constraint on the deployment of visuospatial attention, and, consequently, on the overt scanpath.

The input \mathbf{X} was obtained as follows. For each observer, given the sequence of fixations $\{\mathbf{x}_t\}_{t=1}^{N_T}$, where the vector \mathbf{x}_t represents the fixation position (coordinates) at time t , the amplitude and direction of each gaze shift were computed: $\{l_t, \theta_t\}_{t=1}^{N_T}$. Third feature was the fixation duration $\{f_t\}_{t=1}^{N_T}$.

The random sample $\{l_t, \theta_t, f_t\}_{t=1}^{N_T}$ was summarized through the empirical distribution functions (histograms), that is the random vectors $\mathbf{x}^l = [x_1^l \cdots x_D^l]^T$, $\mathbf{x}^\theta = [x_1^\theta \cdots x_D^\theta]^T$ and $\mathbf{x}^f = [x_1^f \cdots x_D^f]^T$, respectively, where the vector dimension D represents the number of bins of the histogram. The feature vector \mathbf{x}^s is thus a summary of the behavior of a single observer with respect to a particular feature space or source of information $s = 1, \dots, S$, here $S = 3$. Thus, eventually, $\mathbf{X} = \{\mathbf{x}^s\}_{s=1}^S$.

From Figure 33, note that differences between experts and naïve are barely noticeable in terms of features. Clearly, when addressing a scenario in which individual observers are classified as belonging to one or another population, and differences between features are so subtle, more sophisticated ML tools are needed. On this basis, each feature space s was treated as independent and mapped to a specific kernel space (either linear or Gaussian, [72]). Then, the posterior $P(\mathbf{T} | \mathbf{X})$ was rewritten as $P(t_n | \mathbf{x}_n^1, \dots, \mathbf{x}_n^S) = P(t_n | \mathbf{W}, \mathbf{k}_n^\beta)$, where the term on the r.h.s is the Multinomial probit likelihood. Here, $\mathbf{W} \in \mathbb{R}^{N \times C}$ is the matrix of model parameters; the variable \mathbf{k}_n^β is a row of the kernel matrix $\mathbf{K}^\beta \in \mathbb{R}^{N \times N}$ - whose elements are the $K^\beta(\mathbf{x}_i, \mathbf{x}_j)$, i.e. the different kernels - and it expresses how related, based on the selected kernel function,

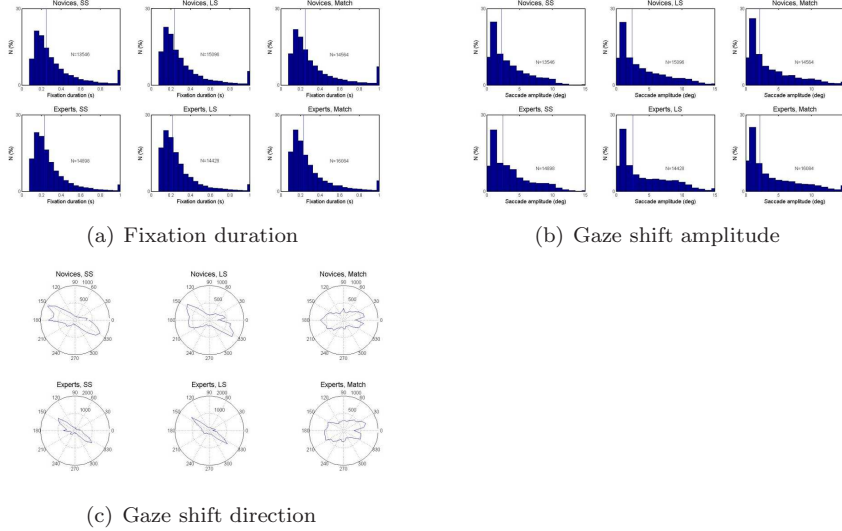


Fig. 33 Empirical distributions (histograms) of $\{t_t, \theta_t, f_t\}_{t=1}^{N_T}$ used to classify expertise. Top panels (33(a)), fixation duration; middle panels (33(b)), gaze shift amplitude; bottom panels (33(c)), gaze shift direction. Vertical solid lines, median values. SS=Short Shots, LS=Long Shots. Modified after [10]

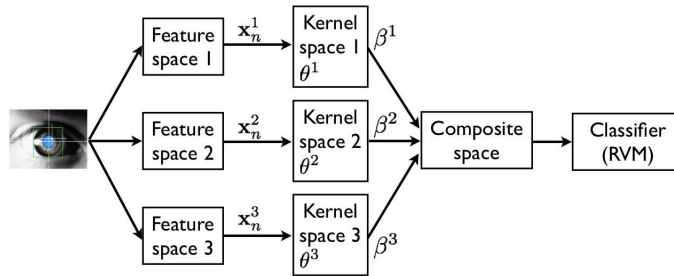


Fig. 34 Data analysis in multiple-kernel representation. The fixation sequence is represented in different feature spaces $s = 1, \dots, S$; each feature \mathbf{x}^s is then separately mapped in a kernel space, each space being generated via kernel K^s of parameters θ^s . The separate kernel spaces are then combined in a composite kernel space, which is eventually used for classification. Modified after [10]

observation \mathbf{x}_n is to the others of the training set. This way (cfr. Figure 34), sources can be combined within a composite kernel space level and classified through a Relevance Vector Machine (RVM), namely a multiple-kernel RVM [83, 28].

Discussing in detail this solution is out of the scope of this chapter (see [10] of a short presentation, and Bishop [3] for more details). However, just to give some hints, RVMs can be considered the Bayesian counterpart of SVMs.

They are Bayesian sparse machines, that is they employ sparse Bayesian learning via an appropriate prior formulation. Not only do they overcome some of the limitations affecting SVMs but also they achieve sparser solutions (and hence they are faster at test time) than SVM. Indeed, by combining only three basic parameters of visual exploration, the overall classification accuracy, expressed as percent correct and averaged across stimulus types and oculomotor features, scored a respectable 78%. More interesting is to consider the best performance for each stimulus type, which testifies the achievement of the classifier, and which depends on the features used. The best performance ranged between 81.90% and 88.09% - 1.852 to 2.399 in terms of d' , which is a quite remarkable result, especially considering that a naturalistic, unconstrained viewing condition was included.

References

1. Aks, D.J., Zelinsky, G.J., Sprott, J.C.: Memory across eye-movements: 1/f dynamic in visual search. *Nonlinear dynamics, psychology, and life sciences* **6**(1), 1–25 (2002)
2. Begum, M., Karray, F., Mann, G., Gosine, R.: A probabilistic model of overt visual attention for cognitive robots. *Systems, Man, and Cybernetics, Part B: Cybernetics, IEEE Transactions on* **40**(5), 1305–1318 (2010)
3. Bishop, C.M.: *Pattern Recognition and Machine Learning (Information Science and Statistics)*. Springer-Verlag New York, Inc., Secaucus, NJ, USA (2006)
4. Boccignone, G., Ferraro, M.: Modelling gaze shift as a constrained random walk. *Physica A: Statistical Mechanics and its Applications* **331**(1-2), 207–218 (2004)
5. Boccignone, G., Ferraro, M.: The active sampling of gaze-shifts. In: G. Maino, G. Foresti (eds.) *Image Analysis and Processing ICIAP 2011, Lecture Notes in Computer Science*, vol. 6978, pp. 187–196. Springer Berlin / Heidelberg (2011)
6. Boccignone, G., Ferraro, M.: Feed and fly control of visual scanpaths for foveation image processing. *annals of telecommunications-Annales des télécommunications* **68**(3-4), 201–217 (2013)
7. Boccignone, G., Ferraro, M.: Gaze shift behavior on video as composite information foraging. *Signal Processing: Image Communication* **28**(8), 949 – 966 (2013)
8. Boccignone, G., Ferraro, M.: Ecological sampling of gaze shifts. *IEEE Trans. on Cybernetics* **44**(2), 266–279 (2014)
9. Boccignone, G., Ferraro, M., Caelli, T.: An information-theoretic approach to active vision. In: *Proceedings 11th International Conference on Image Analysis and Processing, (ICIAP)*, pp. 340–345. IEEE Press (2001)
10. Boccignone, G., Ferraro, M., Crespi, S., Robino, C., de'Sperati, C.: Detecting expert's eye using a multiple-kernel relevance vector machine. *Journal of eye movement research* **7**(2), 1–15 (2014)
11. Boccignone, G., Marcelli, A., Napoletano, P., Di Fiore, G., Iacovoni, G., Morsa, S.: Bayesian integration of face and low-level cues for foveated video coding. *IEEE Transactions on Circuits and Systems for Video Technology* **18**(12), 1727–1740 (2008)
12. Borji, A., Itti, L.: State-of-the-art in visual attention modeling. *IEEE Transactions on Pattern Analysis and Machine Intelligence* **35**(1), 185–207 (2013)
13. Borji, A., Sihite, D.N., Itti, L.: An object-based bayesian framework for top-down visual attention. In: *Twenty-Sixth AAAI Conference on Artificial Intelligence* (2012)
14. Brockmann, D., Geisel, T.: The ecology of gaze shifts. *Neurocomputing* **32**(1), 643–650 (2000)

15. Bundesen, C.: A computational theory of visual attention. *Philosophical Transactions of the Royal Society of London. Series B: Biological Sciences* **353**(1373), 1271–1281 (1998)
16. Cain, M.S., Vul, E., Clark, K., Mitroff, S.R.: A bayesian optimal foraging model of human visual search. *Psychological science* **23**(9), 1047–1054 (2012)
17. Canosa, R.: Real-world vision: Selective perception and task. *ACM Transactions on Applied Perception* **6**(2), 11 (2009)
18. Carpenter, R., Williams, M.: Neural computation of log likelihood in control of saccadic eye movements. *Nature* **377**(6544), 59–62 (1995)
19. Cerf, M., Frady, E., Koch, C.: Faces and text attract gaze independent of the task: Experimental data and computer model. *Journal of Vision* **9**(12) (2009)
20. Cerf, M., Harel, J., Einhäuser, W., Koch, C.: Predicting human gaze using low-level saliency combined with face detection. *Advances in neural information processing systems* **20** (2008)
21. Chambers, J., Mallows, C., Stuck, B.: A method for simulating stable random variables. *J. Am. Stat. Ass.* **71**(354), 340–344 (1976)
22. Chernyak, D.A., Stark, L.W.: Top-down guided eye movements. *IEEE Trans. Systems Man Cybernetics - B* **31**, 514–522 (2001)
23. Chikkerur, S., Serre, T., Tan, C., Poggio, T.: What and where: A bayesian inference theory of attention. *Vision research* **50**(22), 2233–2247 (2010)
24. Clavelli, A., Karatzas, D., Lladós, J., Ferraro, M., Boccignone, G.: Modelling task-dependent eye guidance to objects in pictures. *Cognitive Computation* **6**(3), 558–584 (2014)
25. Codling, E., Plank, M., Benhamou, S.: Random walk models in biology. *Journal of the Royal Society Interface* **5**(25), 813 (2008)
26. Coen-Cagli, R., Coraggio, P., Napoletano, P., Boccignone, G.: What the draughtsman’s hand tells the draughtsman’s eye: A sensorimotor account of drawing. *International Journal of Pattern Recognition and Artificial Intelligence* **22**(05), 1015–1029 (2008)
27. Coen-Cagli, R., Coraggio, P., Napoletano, P., Schwartz, O., Ferraro, M., Boccignone, G.: Visuomotor characterization of eye movements in a drawing task. *Vision research* **49**(8), 810–818 (2009)
28. Damoulas, T., Girolami, M.A.: Combining feature spaces for classification. *Pattern Recognition* **42**(11), 2671–2683 (2009)
29. deCroon, G., Postma, E., van den Herik, H.J.: Adaptive Gaze Control for Object Detection. *Cognitive Computation* **3**, 264–278 (2011)
30. Desimone, R., Duncan, J.: Neural mechanisms of selective visual attention. *Annual review of neuroscience* **18**(1), 193–222 (1995)
31. Dorr, M., Martinetz, T., Gegenfurtner, K., Barth, E.: Variability of eye movements when viewing dynamic natural scenes. *Journal of Vision* **10**(10) (2010)
32. Einhäuser, W., Spain, M., Perona, P.: Objects predict fixations better than early saliency. *Journal of Vision* **8**(14) (2008). DOI 10.1167/8.14.18. URL <http://www.journalofvision.org/content/8/14/18.abstract>
33. Einstein, A.: Zur theorie der brownschen bewegung. *Annalen der Physik* **324**(2), 371–381 (1906)
34. Elazary, L., Itti, L.: A bayesian model for efficient visual search and recognition. *Vision research* **50**(14), 1338–1352 (2010)
35. Ellis, S., Stark, L.: Statistical dependency in visual scanning. *Human Factors: The Journal of the Human Factors and Ergonomics Society* **28**(4), 421–438 (1986)
36. Engbert, R.: Microsaccades: A microcosm for research on oculomotor control, attention, and visual perception. *Progress in brain research* **154**, 177–192 (2006)
37. Engbert, R., Mergenthaler, K., Sinn, P., Pikovsky, A.: An integrated model of fixational eye movements and microsaccades. *Proceedings of the National Academy of Sciences* **108**(39), E765–E770 (2011)

38. Feller, W.: An Introduction to Probability Theory, vol. 1, 2 edn. Wiley, New York (1974)
39. Feng, G.: Eye movements as time-series random variables: A stochastic model of eye movement control in reading. *Cognitive Systems Research* **7**(1), 70–95 (2006)
40. Foulsham, T., Underwood, G.: What can saliency models predict about eye movements? spatial and sequential aspects of fixations during encoding and recognition. *Journal of Vision* **8**(2) (2008)
41. Frintrop, S., Rome, E., Christensen, H.: Computational visual attention systems and their cognitive foundations: A survey. *ACM Trans. on Applied Perception* **7**(1), 6 (2010)
42. Gardiner, C.: Stochastic Methods: A Handbook for the Natural and Social Sciences. Springer Series in Synergetics. Springer-Verlag, Berlin, Heidelberg (2009)
43. Gnedenko, B., Kolmogórov, A.: Limit distributions for sums of independent random variables. Addison-Wesley Pub. Co. (1954)
44. Hacısalihzade, S., Stark, L., Allen, J.: Visual perception and sequences of eye movement fixations: A stochastic modeling approach. *IEEE Trans. Syst., Man, Cybern.* **22**(3), 474–481 (1992)
45. Haji-Abolhassani, A., Clark, J.J.: A computational model for task inference in visual search. *Journal of vision* **13**(3), 29 (2013)
46. Heinke, D., Backhaus, A.: Modelling visual search with the selective attention for identification model (vs-saim): a novel explanation for visual search asymmetries. *Cognitive computation* **3**(1), 185–205 (2011)
47. Heinke, D., Humphreys, G.W.: Attention, spatial representation, and visual neglect: simulating emergent attention and spatial memory in the selective attention for identification model (saim). *Psychological review* **110**(1), 29 (2003)
48. Heinke, D., Humphreys, G.W.: Computational models of visual selective attention: A review. *Connectionist models in cognitive psychology* **1**(4), 273–312 (2005)
49. Henderson, J.M., Shinkareva, S.V., Wang, J., Luke, S.G., Olejarczyk, J.: Predicting cognitive state from eye movements. *PLoS ONE* **8**(5), e64,937 (2013)
50. Hills, T.T.: Animal foraging and the evolution of goal-directed cognition. *Cognitive Science* **30**(1), 3–41 (2006)
51. Ho Phuoc, T., Guérin-Dugué, A., Guyader, N.: A computational saliency model integrating saccade programming. In: Proc. Int. Conf. on Bio-inspired Systems and Signal Processing, pp. 57–64. Porto, Portugal (2009)
52. Horowitz, T., Wolfe, J.: Visual search has no memory. *Nature* **394**(6693), 575–577 (1998)
53. Huang, K.: Introduction to statistical physics. CRC Press, Boca Raton, FL (2001)
54. Humphreys, G.W., Muller, H.J.: Search via recursive rejection (serr): A connectionist model of visual search. *Cognitive Psychology* **25**(1), 43–110 (1993)
55. Itti, L., Koch, C., Niebur, E.: A model of saliency-based visual attention for rapid scene analysis. *IEEE Transactions on Pattern Analysis and Machine Intelligence* **20**, 1254–1259 (1998)
56. Jaynes, E.T.: Probability theory: the logic of science. Cambridge University Press, New York, NY (2003)
57. Keech, T., Resca, L.: Eye movements in active visual search: A computable phenomenological model. *Attention, Perception, & Psychophysics* **72**(2), 285–307 (2010)
58. Kimura, A., Pang, D., Takeuchi, T., Yamato, J., Kashino, K.: Dynamic markov random fields for stochastic modeling of visual attention. In: Proc. ICPR '08., pp. 1–5. IEEE (2008)
59. Koch, C., Ullman, S.: Shifts in selective visual attention: towards the underlying neural circuitry. *Human Neurobiology* **4**(4), 219–27 (1985)
60. Koller, D., Friedman, N.: Probabilistic graphical models: principles and techniques. MIT press, Cambridge, MA (2009)
61. Koutrouvelis, I.: Regression-type estimation of the parameters of stable laws. *Journal of the American Statistical Association* pp. 918–928 (1980)

62. Lagun, D., Manzanares, C., Zola, S.M., Buffalo, E.A., Agichtein, E.: Detecting cognitive impairment by eye movement analysis using automatic classification algorithms. *Journal of Neuroscience Methods* **201**(1), 196–203 (2011)
63. Logan, G.D.: The code theory of visual attention: an integration of space-based and object-based attention. *Psychological review* **103**(4), 603 (1996)
64. MacKay, D.: *Information Theory, Inference and Learning Algorithms*. Cambridge University Press, Cambridge, UK (2002)
65. Makarava, N., Bettenbühl, M., Engbert, R., Holschneider, M.: Bayesian estimation of the scaling parameter of fixational eye movements. *EPL* **100**(4), 40,003 (2012)
66. Mantegna, R.N., Stanley, H.E., et al.: *An introduction to econophysics: correlations and complexity in finance*. Cambridge University Press, Cambridge, UK (2000)
67. Marat, S., Rahman, A., Pellerin, D., Guyader, N., Houzet, D.: Improving visual saliency by adding face feature map and center bias. *Cognitive Computation* **5**(1), 63–75 (2013)
68. Marr, D.: *Vision: A Computational Investigation into the Human Representation and Processing of Visual Information*. W.H. Freeman, New York (1982)
69. Martinez-Conde, S., Otero-Millan, J., Macknik, S.L.: The impact of microsaccades on vision: towards a unified theory of saccadic function. *Nature Reviews Neuroscience* **14**(2), 83–96 (2013)
70. Méndez, V., Campos, D., Bartumeus, F.: *Stochastic Foundations in Movement Ecology: Anomalous Diffusion, Front Propagation and Random Searches*. Springer Series in Synergetics. Springer-Verlag, Berlin, Heidelberg (2014)
71. Mozer, M.C.: *Early parallel processing in reading: A connectionist approach*. Lawrence Erlbaum Associates, Inc (1987)
72. Murphy, K.P.: *Machine learning: a probabilistic perspective*. MIT press, Cambridge, MA (2012)
73. Najemnik, J., Geisler, W.: Optimal eye movement strategies in visual search. *Nature* **434**(7031), 387–391 (2005)
74. Napoletano, P., Boccignone, G., Tisato, F.: Attentive monitoring of multiple video streams driven by a bayesian foraging strategy. *IEEE Trans. on Image Processing* **24**(11), 3266–3281 (2015)
75. Nolan, J.: Numerical calculation of stable densities and distribution functions. *Communications in Statistics-Stochastic Models* **13**(4), 759–774 (1997)
76. Otero-Millan, J., Macknik, S.L., Langston, R.E., Martinez-Conde, S.: An oculomotor continuum from exploration to fixation. *Proceedings of the National Academy of Sciences* **110**(15), 6175–6180 (2013)
77. Over, E., Hooge, I., Vlaskamp, B., Erkelens, C.: Coarse-to-fine eye movement strategy in visual search. *Vision Research* **47**, 2272–2280 (2007)
78. Palmer, J., Verghese, P., Pavel, M.: The psychophysics of visual search. *Vision research* **40**(10), 1227–1268 (2000)
79. Paul, W., Baschnagel, J.: *Stochastic Processes: From Physics to Finance*. Springer International Publishing, Berlin, Heidelberg (2013)
80. Phaf, R.H., Van der Heijden, A., Hudson, P.T.: Slam: A connectionist model for attention in visual selection tasks. *Cognitive Psychology* **22**(3), 273–341 (1990)
81. Plank, M., James, A.: Optimal foraging: Lévy pattern or process? *Journal of The Royal Society Interface* **5**(26), 1077 (2008)
82. Moscoso del Prado Martin, F.: A theory of reaction time distributions (2008). URL <http://cogprints.org/6310/1/recinormal.pdf>
83. Psorakis, I., Damoulas, T., Girolami, M.A.: Multiclass relevance vector machines: sparsity and accuracy. *IEEE Transactions on Neural Networks* **21**(10), 1588–1598 (2010)
84. Ramos-Fernandez, G., Mateos, J., Miramontes, O., Cocho, G., Larralde, H., Ayala-Orozco, B.: Lévy walk patterns in the foraging movements of spider monkeys (*Ateles geoffroyi*). *Behavioral Ecology and Sociobiology* **55**(3), 223–230 (2004)

85. Rao, R.P., Zelinsky, G.J., Hayhoe, M.M., Ballard, D.H.: Eye movements in iconic visual search. *Vision Research* **42**(11), 1447 – 1463 (2002)
86. Ratcliff, R., McKoon, G.: The diffusion decision model: Theory and data for two-choice decision tasks. *Neural computation* **20**(4), 873–922 (2008)
87. Rensink, R.: The dynamic representation of scenes. *Visual Cognition* **1**(3), 17–42 (2000)
88. Reynolds, A.: How many animals really do the Lévy walk? Comment. *Ecology* **89**(8), 2347–2351 (2008)
89. Reynolds, A.: Optimal random Lévy-loop searching: New insights into the searching behaviours of central-place foragers. *EPL (Europhysics Letters)* **82**, 20,001 (2008)
90. Rogers, S., Girolami, M.: A first course in machine learning. CRC Press (2011)
91. Rutishauser, U., Koch, C.: Probabilistic modeling of eye movement data during conjunction search via feature-based attention. *Journal of Vision* **7**(6) (2007)
92. Scholl, B.: Objects and attention: the state of the art. *Cognition* **80**(1-2), 1–46 (2001)
93. Schütz, A., Braun, D., Gegenfurtner, K.: Eye movements and perception: A selective review. *Journal of Vision* **11**(5) (2011)
94. Siegert, S., Friedrich, R.: Modeling of nonlinear Lévy processes by data analysis. *Physical Review E* **64**(4), 041,107 (2001)
95. Stephen, D., Mirman, D., Magnuson, J., Dixon, J.: Lévy-like diffusion in eye movements during spoken-language comprehension. *Physical Review E* **79**(5), 056,114 (2009)
96. Sun, Y., Fisher, R., Wang, F., Gomes, H.M.: A computer vision model for visual-object-based attention and eye movements. *Computer Vision and Image Understanding* **112**(2), 126 – 142 (2008)
97. Tatler, B.: The central fixation bias in scene viewing: Selecting an optimal viewing position independently of motor biases and image feature distributions. *Journal of Vision* **7**(14) (2007)
98. Tatler, B., Baddeley, R., Vincent, B.: The long and the short of it: Spatial statistics at fixation vary with saccade amplitude and task. *Vision research* **46**(12), 1857–1862 (2006)
99. Tatler, B., Hayhoe, M., Land, M., Ballard, D.: Eye guidance in natural vision: Reinterpreting salience. *Journal of vision* **11**(5) (2011)
100. Tatler, B., Vincent, B.: Systematic tendencies in scene viewing. *Journal of Eye Movement Research* **2**(2), 1–18 (2008)
101. Tatler, B., Vincent, B.: The prominence of behavioural biases in eye guidance. *Visual Cognition* **17**(6-7), 1029–1054 (2009)
102. Torralba, A.: Contextual priming for object detection. *Int. J. of Comp. Vis.* **53**, 153–167 (2003)
103. Treisman, A.: Feature binding, attention and object perception. *Philosophical Transactions of the Royal Society of London. Series B: Biological Sciences* **353**(1373), 1295–1306 (1998)
104. Treisman, A.M., Gelade, G.: A feature-integration theory of attention. *Cognitive psychology* **12**(1), 97–136 (1980)
105. Trillenber, P., Gross, C., Shelhamer, M.: Random walks, random sequences, and nonlinear dynamics in human optokinetic nystagmus. *Journal of Applied Physiology* **91**(4), 1750–1759 (2001)
106. Van Der Linde, I., Rajashekar, U., Bovik, A.C., Cormack, L.K.: Doves: a database of visual eye movements. *Spatial vision* **22**(2), 161–177 (2009)
107. Van Kampen, N.G.: Stochastic processes in physics and chemistry. North Holland, Amsterdam, NL (2001)
108. Viswanathan, G., Raposo, E., da Luz, M.: Lévy flights and superdiffusion in the context of biological encounters and random searches. *Physics of Life Rev.* **5**(3), 133–150 (2008)

109. Viswanathan, G.M., Da Luz, M.G., Raposo, E.P., Stanley, H.E.: The physics of foraging: an introduction to random searches and biological encounters. Cambridge University Press, Cambridge, UK (2011)
110. Walther, D., Koch, C.: Modeling attention to salient proto-objects. *Neural Networks* **19**(9), 1395–1407 (2006)
111. Wischnewski, M., Belardinelli, A., Schneider, W., Steil, J.: Where to Look Next? Combining Static and Dynamic Proto-objects in a TVA-based Model of Visual Attention. *Cognitive Computation* **2**(4), 326–343 (2010)
112. Wolfe, J.M.: Guided search 2.0 a revised model of visual search. *Psychonomic bulletin & review* **1**(2), 202–238 (1994)
113. Wolfe, J.M.: When is it time to move to the next raspberry bush? foraging rules in human visual search. *Journal of vision* **13**(3), 10 (2013)
114. Yarbus, A.: *Eye Movements and Vision*. Plenum Press, New York (1967)
115. Zelinsky, G.J.: A theory of eye movements during target acquisition. *Psychological review* **115**(4), 787 (2008)